RESEARCH ARTICLE

ESPL WILEY

Landscape evolution during Holocene transgression of a mid-latitude low-relief coastal plain: The southern North Sea

Stephen Eaton[1] | Natasha L. M. Barlow[1] | David M. Hodgson[1] |
Claire L. Mellett[1,2] | Andy R. Emery[3]

[1]School of Earth and Environment, University of Leeds, Leeds, UK

[2]Royal HaskoningDHV, London, UK

[3]Wessex Archaeology, Salisbury, UK

Correspondence
Natasha L. M. Barlow, School of Earth and Environment, University of Leeds, LS2 9JT, Leeds, UK.
Email: n.l.m.barlow@leeds.ac.uk

Present address
Stephen Eaton, ARUP, London, UK.

Abstract

Low-relief coastal landscapes are at major risk of rising sea levels, as vertical changes in relative sea level have far-reaching lateral effects. Integration of a dense 2D grid of seismic reflection data with sedimentological and geotechnical data obtained in two offshore wind farm zones allows detailed documentation of postglacial landforms and environmental change over a 1,021 km^2 area in the western sector of the southern North Sea. Following the retreat of Last Glacial Maximum ice sheets from the southern North Sea, the resulting postglacial terrestrial landscape provided a surface for peatland formation as climate started to warm and the water table rose in response to relative sea-level rise. Southward-draining fluvial networks formed contemporaneously with the peatlands, and remnants of this terrestrial wetland landscape are buried beneath Holocene marine sediments. Distinctive isolated incisional features and discrete widening of fluvial channels that cut through the peats are interpreted as either tidal ponds or relict tidal channels. These features record the evolution of this landscape through the Early Holocene as marine transgression inundated a low-relief coastal plain. The erosion of the peatlands observed in the cores, the patchy preservation of the organic wetland landscape, and the lack of preserved barrier systems recorded by the seismic reflection data suggest that the rate of relative sea-level rise outpaced sediment supply during the Late Postglacial and Early Holocene in this area of the southern North Sea. In a regional context, the southward draining river channels contrast to northward fluvial drainage to the North Sea, pointing to a subtle drainage divide in the palaeolandscape and the presence of a low-relief land bridge separating the North Sea and the English-Channel/La Manche during the Early Holocene. The documented scenario of rising sea levels combined with decreasing sediment supply in a low-relief setting is a situation faced by many global deltas and coastlines, which makes the southern North Sea a crucial archive of coastal landscape change.

KEYWORDS
coast, Holocene, North Sea, offshore wind, postglacial, sea level, sediment supply, seismic, submerged landforms

1 | INTRODUCTION

Low-relief coastal landscapes are at high risk of rising sea levels, as vertical changes in relative sea level (RSL) have far-reaching lateral effects. Observational data of coastal landscape response to the magnitude of sea-level rise predicted for the coming centuries is limited (Nienhuis et al., 2023). Therefore, reconstructions of low-relief Holocene coastlines have the potential to inform understanding of coastal landscape response to changing RSL (e.g., McGowan & Baker, 2014).

The environmental evolution of low-relief coastal plains is a consequence of the complicated interplay between hydrodynamics, coastal morphology, sediment supply, accommodation and the rate of RSL change (Passeri et al., 2015). Many onshore studies are based in locations with high Holocene sediment input, including the Mississippi; the Yangtze River Delta; the Humber and the Rhine and Wadden Sea (Darby et al., 2020; Karle et al., 2021; Shennan et al., 2003; Tornqvist, 1993; Yu et al., 2012), which have the potential to keep up with, or outpace, the rate of RSL rise (Syvitski, Harvey, et al., 2005). These are atypical of modern coastal plains, where anthropogenic activities have restricted sediment input by damming rivers upstream or sand mining (Blum & Roberts, 2009; Bussi et al., 2021; Hackney et al., 2021; Yang et al., 2005). Palaeo low-relief landscapes with low sediment supply subjected to marine transgression are rarely documented. Examples of low-relief landscapes where increases in accommodation outpace sediment supply due to rising sea levels could provide important constraints on coastal response to changing sea levels and hydrodynamics. In addition, for valid logistical reasons, many studies into Holocene coastal landscapes are limited to coastal exposures or disparate boreholes (e.g., Hijma & Cohen, 2011) or ground-penetrating radar restricted to locations above the limit of saline influence (e.g., Bristow et al., 2000), requiring interpolation between locations to reconstruct palaeogeographic configurations.

To overcome these challenges, we utilise data collected by the offshore wind industry to develop a detailed temporal and spatial reconstruction over >1,000 km^2 of a now-submerged Holocene low-relief coastal landscape, presenting an example of the evolution of a low-relief and low sediment-supply coastal landscape to changing climate and RSL during the Early Holocene.

2 | SETTING AND METHODOLOGY

The density of seismic reflection data (gridline spacing as close as 100 m) required for offshore windfarm ground models allows the development of pseudo-3D reconstructions of Quaternary landscapes, calibrated by borehole records and cone-penetration tests, to reconstruct the changing glacial-terrestrial–marine environment in the North Sea (Cartelle et al., 2021; Cotterill et al., 2017; Emery et al., 2019). We use a seismic reflection and borehole dataset, integrating palaeoenvironmental data and radiocarbon dates with geophysical analysis, from wind farms offshore East Anglia, UK, to develop a model of the Late Glacial and Holocene stratigraphic record, from a warming postglacial landscape colonised by freshwater terrestrial peatlands, subsequently transgressed by marine sediments under rising RSL.

2.1 | Setting

The Norfolk Vanguard (NV) West and Norfolk Boreas offshore wind farm zones are located c.50 km east of the East Anglian coastline (Figure 1) in the southern North Sea. In total, the study area covers approximately 1,021 km^2, in <50 m water depth, with major variations
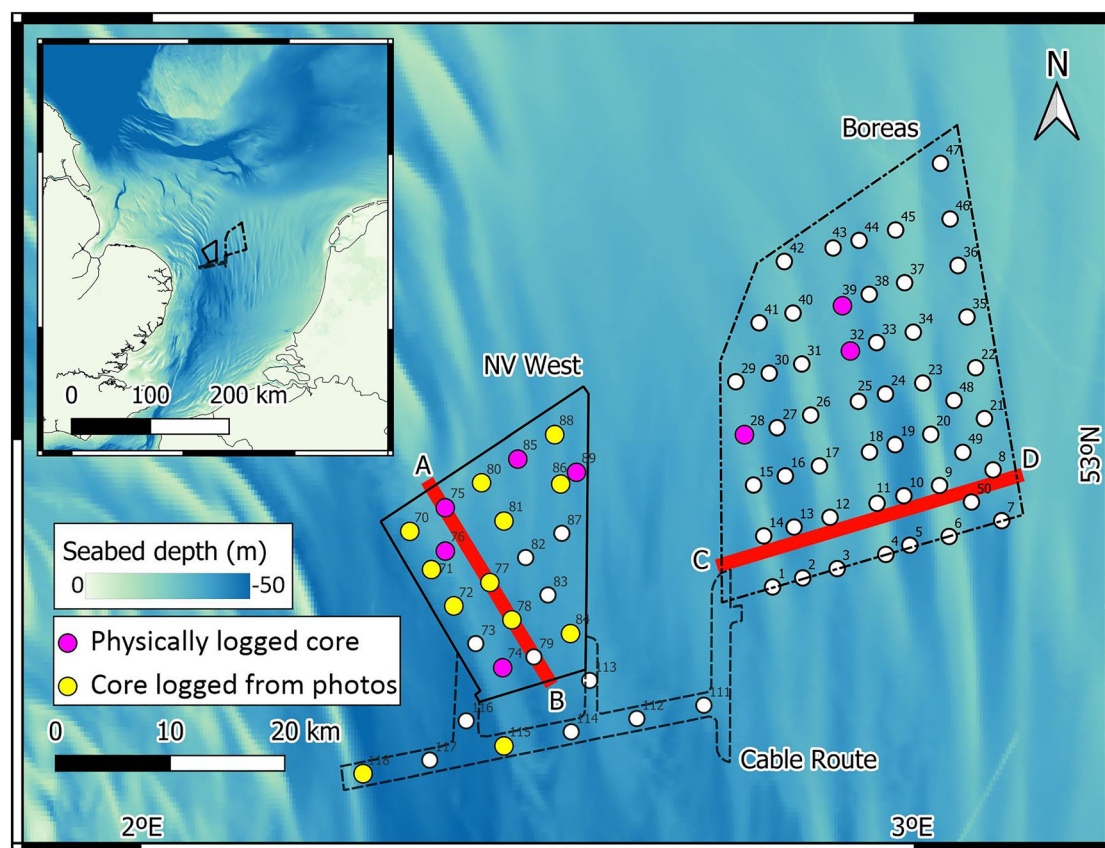
FIGURE 1 Norfolk Vanguard (NV) West and Norfolk Boreas survey areas with locations and names of 79 paired vibrocores and cone penetration test (CPT) sites. Background bathymetry map utilises the regional GEBCO 2023 grid (GEBCO, 2023). Red lines indicate the locations of the panels shown in Figure 2. [Color figure can be viewed at wileyonlinelibrary.com]

in bathymetry due to north–south trending sandbanks (Figure 1). The Last Glacial period (regionally termed Devensian) top surface is underlain by low-energy estuarine silts and clays of the Brown Bank Formation (MIS 5d–4) that erosionally overly deposits of the Yarmouth Roads (which most likely corresponds to MIS 19–13) and Swarte Bank (MIS12) formations, which are reported in detail in Eaton et al. (2020). Currently, there are a limited number of sea-level index points from which to constrain the elevation and rate of RSL change in the region since the Last Glacial Maximum (LGM) (Shennan et al., 2018; Shennan & Andrews, 2000). However, recent modelling of changes in seabed depths shows that the elevation of this region of the southern North Sea was ∼50 m above modern sea level c. 15 ka due to the solid Earth response to mass loading by the nearby British-Irish Ice Sheet during the Last Glacial period. From 15 ka to the present, RSL then rose due to the melting of far-field ice sheets and glacio-isostatic adjustment in response to the melting of the British-Irish Ice Sheet resulting in a fall in the relative elevation of the land surface during the Early Holocene and subsequent flooding of the North Sea by 8 ka (Bradley et al., 2023; Clark et al., 2022).

2.2 | Seismic reflection data

A hull-mounted Pinger (Massa TR-1075 Pinger array), and a towed multichannel Ultra-High-Resolution (UHR) seismic reflection system were used to image the shallow subsurface of the study area by Fugro, on behalf of Vattenfall Wind Power UK. The Pinger seismic reflection data has a depth of investigation down to ∼30 m below the seabed and uses a relatively high frequency (4.5 kHz), equating to a vertical resolution of 0.1–0.2 m. The UHR seismic reflection data was acquired with a sparker source, which is higher energy than the Pinger and therefore achieved a greater depth of penetration (up to ∼300 m) with a frequency of 4 Hz, which equates to a vertical resolution of 1 m immediately below the seabed and 5 m at 300 m with an approximately linear decrease with depth. The UHR and Pinger seismic reflection data had been depth converted by Fugro Oceansismica SpA prior to analysis by the authors. A seismic velocity of 1,600 m s^{-1} was used for the Pinger seismic reflection data to convert from two-way travel time (TWTT) to depths in metres, and the UHR seismic reflection data was depth converted using a velocity field derived during seismic processing. The appropriateness of the seismic velocity used for depth conversion was confirmed by a good fit between the cone penetration test profiles and the depth-converted sections.

Seismic reflection data has been interpreted on every available inline and x-line by the authors using IHS Kingdom software with characterisation of seismic facies and stratigraphy following Michum et al. (1977) and Mellett et al. (2013). Interpreted seismic surfaces were gridded using a minimum curvature algorithm, which provides geologically plausible surfaces. The cell size used for gridding was specified based on the data resolution (25 × 25 m for UHR and 20 × 20 m for Pinger) so that no more than one point from each cell contributes to a mapped seismic surface. For the purposes of this study, Pinger data has been used primarily to interpret stratigraphic and geomorphological features. In cases where the Pinger seismic reflection data were not of sufficient quality (poor imaging), the UHR seismic reflection data have been used.

2.3 | Bathymetry data

Site-specific multibeam echo sounder (MBES) bathymetric data were acquired using a Kongsberg EM 2040, with a frequency of 400 kHz. A regional MBES survey was acquired in 2010 that achieved approximately 31% coverage, whilst in 2015 (NV West and associated Export Cable Route) and 2017 (Norfolk Boreas) full coverage MBES surveys were acquired. The projected coordinate system used for these surveys is ETRS89/UTM zone 31 N (EPSG: 25831).

2.4 | Vibrocores and palaeoenvironmental data

Sedimentological changes were logged in detail in eight cores (VCs 28, 32, 39, 74, 75, 76, 85 and 89) (marked in Figure 1) made available to Wessex Archaeology as part of the windfarm archaeological assessment. We recorded changes in grain size using a grain-size comparator card, visual estimates of sorting, textural changes (brittle, friable, plastic) and colour according to the Munsell colour scale, as well as changes in sedimentary structures, and the presence of plant remains or shells. The core observations were used to build sedimentary facies, which were assigned sedimentary facies codes. In addition, 12 cores were logged using high-resolution photographs (VCs 70, 71, 72, 77, 78, 80, 81, 84, 86, 88, 115 and 118) to support the identification of stratigraphic boundaries and sedimentary facies. The palaeoenvironmental interpretation of the units was supported by microfossil analysis and radiocarbon dates reported by Wessex Archaeology (2019a, 2019b). We re-calibrated the radiocarbon dates with IntCal20 (Reimer et al., 2020) and reported the 2-sigma range (Table 1).

2.5 | Cone penetration tests

Seventy-nine Cone Penetration Tests (CPTs) were acquired as part of the NV West and Norfolk Boreas site surveys, taken at the same locations as the vibrocores (Figure 1). CPTs sampled to a maximum depth of 50 m below the seabed in the NV West and Norfolk Boreas survey areas, and down to a maximum of 7 m below the seabed in the Export Cable Route survey area. The CPT measurements of cone resistance (qc) and sleeve friction (fs) have been used to derive the friction ratio (Rf). The friction ratio has been used here as an indicator of soil/sediment type (grain size). Although no firm interpretation of sedimentary facies can be made from CPT logs, depositional environments can be determined when correlated with seismic facies and lithofacies from the vibrocores.

3 | RESULTS

3.1 | Seismic stratigraphic interpretation

Eaton et al. (2020) subdivided the Middle to Late Pleistocene seismic stratigraphy in the study area into four seismic units (L1–4) based on seismically mapped erosional surfaces/contacts (S1–4) that separate distinct seismic facies associations. Eaton et al. (2020) focussed on

TABLE 1 Details of radiocarbon dates and 2-sigma age ranges calibrated by IntCal20 (Reimer et al., 2020) for samples taken by Wessex Archaeology (original source report given in final column) to constrain the ages of the peats in six vibrocores shown in Figure 10. Latitude and longitude of each vibrocore location are provided alongside the core codes. Note radiocarbon samples marked * are considered reworked or unreliable by Wessex Archaeology. No depth uncertainties (m LAT) and limited ^{14}C sample thickness uncertainties are given in the original publications.

Laboratory code	Depth, meters below sea floor (m LAT)	14C age ± error (BP)	2-sigma calibrated age range (cal. BP)	Sample position	Material dated	Wessex archaeology report data source
VC074 (52°49′32.3431"N 002°27′56.612"E)						
UB-36846	0.90 (−39.40)	8,955 ± 46	10,227–9,909	Top of peat	Seeds (*Nuphar lutea* 2x, *Nymphaea alba* 2x, Juncus sp. 1x, Cyperaceae 1/2x) + leaves (Sphagnum sp. 25x)	2018b
UBA-39469 *	1.18 (−39.68)	9,696 ± 44	11,228–10,808	Mid peat	Seeds (Cyperaceae, Solanum sp. and Alisma sp) + Poaceae husks	2019b
UBA-39470 *	1.45 (−39.95)	9,613 ± 39	11,172–10,773	Mid peat	Seeds (Juncus sp., Betula sp., Caryophyllaceae, Alisma sp., Chenopodiaceae and Carex sp.)	2019b
UB-36847	1.56 (−40.06)	9,122 ± 49	10,483–10,199	Base of peat	Seeds (Betula sp. 3x, Solanum sp. 2x, Chenopodium sp. 1x, Caryophyllaceae 1x, Betula sp. 5x, *Lycopus europaeus* 1x, Potamogeton sp. 1x, *N. alba* 1x, Cyperaceae 15x) + Betula sp. catkin scale 1x	2018b
VC076 (52°55′00.0131"N 002°23′24.916"E)						
UB-36848	3.61–3.63 (−37.61 to −37.93)	8,936 ± 47	10,210–9,903	Top of peat	Seeds (*L. europaeus* 1x, Juncus sp 2x, Asteraceae 1x, Carex sp 2x., Ranunculus sp. 0.5)	2018b
UB-36849	3.91–3.93 (−37.91 to −37.93)	11,863 ± 55	13,982–13,521	Base of peat	Seeds (Potamogeton sp. 5x)	2018b
VC085 (52°59′21.0594"N 002°29′00.041"E)						
UB-36850 *	1.75–1.77 (−37.15 to −37.17)	10,192 ± 47	12,001–11,645	Top peat	Seeds (Ceratophyllum sp. 1x, *Menyanthes trifoliata* 2x)	2018b
UB-36851	2.07–2.09 (−37.47 to −37.49)	8,856 ± 48	10,172–9,736	Base of peat	Seeds (*M. trifoliata* 2x)	2018b
VC028 (53°00′32.7348"N 002°46′43.018″E)						
UBA-38188	2.59–2.62 (−33.79 to −33.82)	8,749 ± 40	9,894–9,555	Mid peat	Bud scales	2018a
VC032 (53°04′30.0324"N 002°54′57.949″E)						
UBA-39473 *	3.61 (−35.51)	9,124 ± 77	10,506–10,175	Upper intertidal clays	Organic material with Sphagum leaves	2019a
UBA-38189	3.83 (−35.73)	8,697 ± 45	9,887–9,542	Top of peat	*M. trifoliata* seed	2018a
UBA-39474	3.95 (−35.85)	8,894 ± 78	10,211–9,710	Mid peat	Lamiaceae, Ranunculus sp., *M. trifoliata* seeds	2019a
UBA-38190	4.11 (−36.01)	9,992 ± 51	11,709–11,263	Base of peat	Bulk organic sediment (sample thickness not stated)	2018a
VC039 (53°06′37.0224"N 002°54′21.938″E)						
UBA-39471	2.96 (−35.65)	8,510 ± 58	9,553–9,334	Top of peat	*M. trifoliata* seed	2019b
UBA-38191 *	3.07 (−35.77)	10,881 ± 60	12,917–12,728	Base of peat	*M. trifoliata* seed	2018a
UBA-39472	3.13 (−35.83)	10,435 ± 66	12,616–12,004	Top of fluvial unit	*M. trifoliata*, Betula sp., Characeae oospores, Typha sp.	2019b

the documentation of L4 (Yarmouth Roads Fm.), L3 (Swarte Bank Fm.) and L2 (Brown Bank Fm.) and their bounding surfaces (Surface 4, Surface 3 and Surface 2). This paper focuses on the composite Surface 1 (S1) and the overlying seismic unit, L1, which comprises the channel-fill unit (CFU), the seismic anomaly unit (SAU), the incisional-fill unit (IU), and the seabed bedforms (SB) unit (Figure 2).
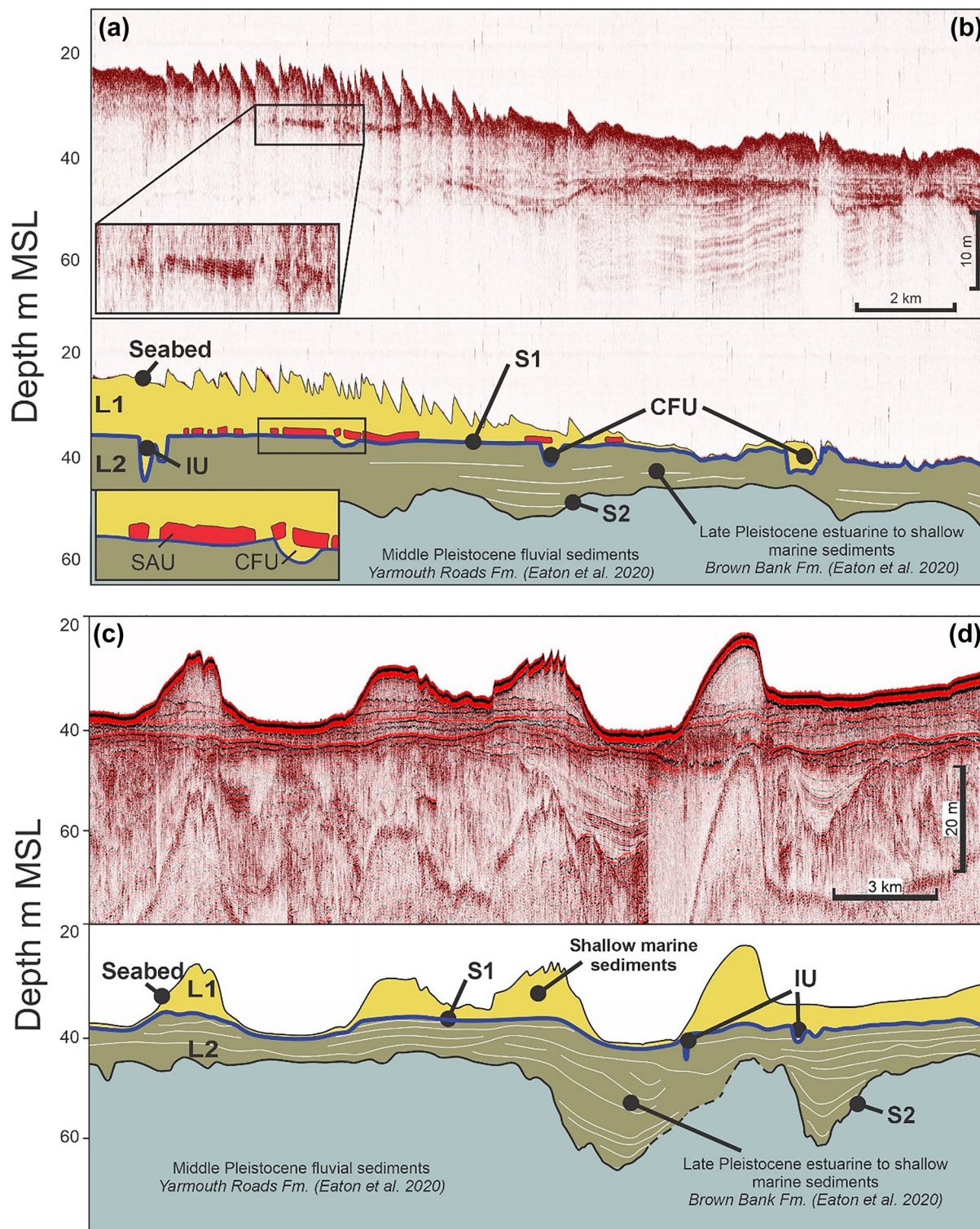
FIGURE 2 Seismic reflection profile and interpreted panels illustrating seismic stratigraphic units and surfaces. Panel (a-b) shows an example seismic line (Pinger) through NV West (~200x vertical exaggeration). Seismic unit L1 is associated with sand banks and shallow marine sediments. Where L1 is not identified, only a thin veneer (<20 cm thick) of shallow marine sand covers the Late Pleistocene sediments. Panel (c-d) shows an example seismic line through Boreas (~150x vertical exaggeration). The north–south trending sand banks are clearly visible with Late Pleistocene sediments cropping out in between. For the location of seismic reflection profiles see Figure 1. S1 = surface 1, S2 = surface 2, L1 = seismic unit 1, L2 = seismic unit 2, SAU = seismic anomaly unit, CFU = channel-fill unit, IU = incised unit. [Color figure can be viewed at wileyonlinelibrary.com]

3.1.1 | Surface 1 (S1)

Surface 1 (S1) is mapped across the entire study area (Figure 3) and is ornamented with channel-forms and incisional features. In the underlying L2 unit (Eaton et al., 2020), seismic reflectors are sub-parallel to, and truncated by, S1. In some areas, S1 loses reflectivity

and is only distinguishable by stratigraphic change in seismic facies between the underlying L2 and overlying L1 sub-units. The overlying seismic unit 1 (L1) is characterised by both high-amplitude, low-frequency seismic reflectors, and low-amplitude, low-frequency seismic reflectors, but is distinguishable from the underlying units by changes in seismic reflector amplitude and seismic facies character,
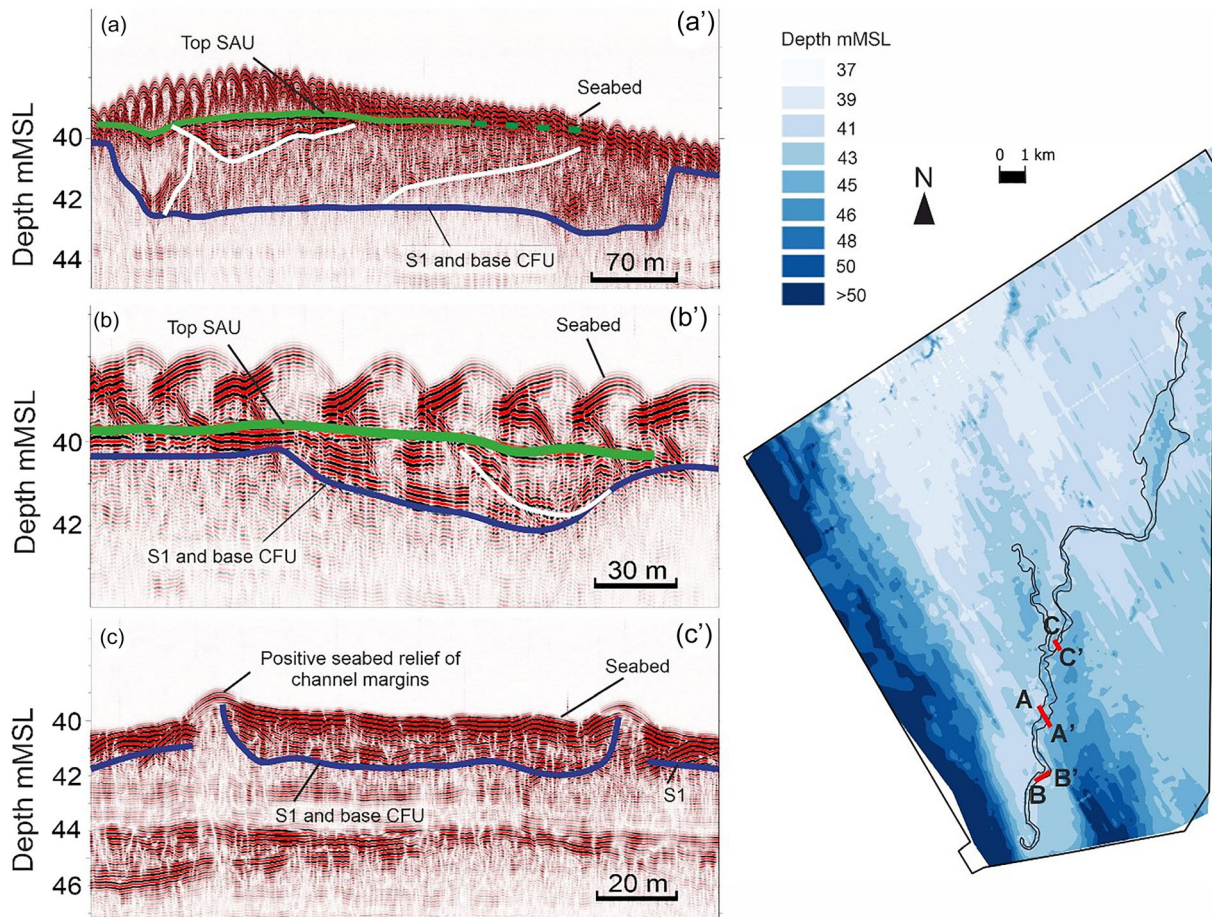
FIGURE 3 A range of seismic fill types characterise the channel-fill unit (CFU). (a) CFU with cut-and-fill architecture and the seismic anomaly unit (SAU) partially overlying the fill. The SAU is not present on the margins, though does extend to the seabed (dotted green line). (b) CFU-fill example with high amplitude basal bounding seismic reflectors, and cut-and-fill architecture. The SAU overlies the CFU and is present on the southern margin. (c) The CFU with no overlying SB and visible on the seabed with positive relief. (d) Depth map (m MSL) of the surface 1 (S1) in NV West with locations of panels (a), (b), (c). [Color figure can be viewed at wileyonlinelibrary.com]

and aids in the mapping of S1 (Figure 2). Crosscutting erosional surfaces indicate that S1 is a composite erosion surface.

3.1.2 | Seismic unit 1 (L1)

The base of L1 is defined by S1, and the top is constrained by the modern seabed. The seismic character of L1 is highly variable across both areas and ranges from diffuse to reflective. The thicker L1 deposits are typically located where thick shallow marine sediments are present, often with multi-meter scale variations in seabed topography indicative of sedimentary bedforms. Where S1 is coincident with the seabed, either the L1 unit is not present or considered below the resolution of the seismic reflection data. L1 is a composite of four subunits: the channel-fill seismic unit (CFU), a seismic anomaly unit (SAU), the incision-fill seismic unit (IU) and the seabed bedforms unit (SB) (Figure 2).

3.1.3 | Channel-fill seismic unit (CFU)

The base of the channel-fill seismic unit (CFU) forms part of the composite S1 surface and is defined by the contrast in seismic facies between the CFU and the underlying L2 unit (Eaton et al., 2020). The

basal incision surface lies ~40 m below mean sea level (MSL) and is clearly imaged in the UHR seismic. The fill, characterised by a range of seismic facies seen in the higher frequency Pinger seismic reflection data, shows a range of architectural styles, although where overlain by thick (>3 m) shallow marine sediments (SB unit) the CFU has less reflectivity due to absorption of the signal. Where L1 is <0.5 m thick, the top of the CFU is characterised by high-amplitude, low-frequency seismic reflectors. In the southwest of the study area, the CFU is typically composed of stacked channel-fills (cut-and-fill seismic character), and dipping and draped reflectors (Figure 3a,b). In the northeast, the seismic character of the CFU fill is dominated by parallel, sub-horizontal and draped seismic reflectors (Figure 3d and Figure 4). Within the central area of NV West, the CFU is exposed at the seabed and can be mapped using multibeam bathymetry data. The CFU at the seabed has a positive relief (up to 2 m) compared with the surrounding seabed and a sinuous planform (Figure 3c).

3.1.4 | Seismic anomaly unit (SAU)

The seismic anomaly unit (SAU) conformably overlies S1 in NV West and Norfolk Boreas and has a patchy spatial distribution (Figure 5). In some locations, the SAU abruptly terminates, without clear evidence of incision by channels (Figure 5a). The SAU either overlies the CFU,
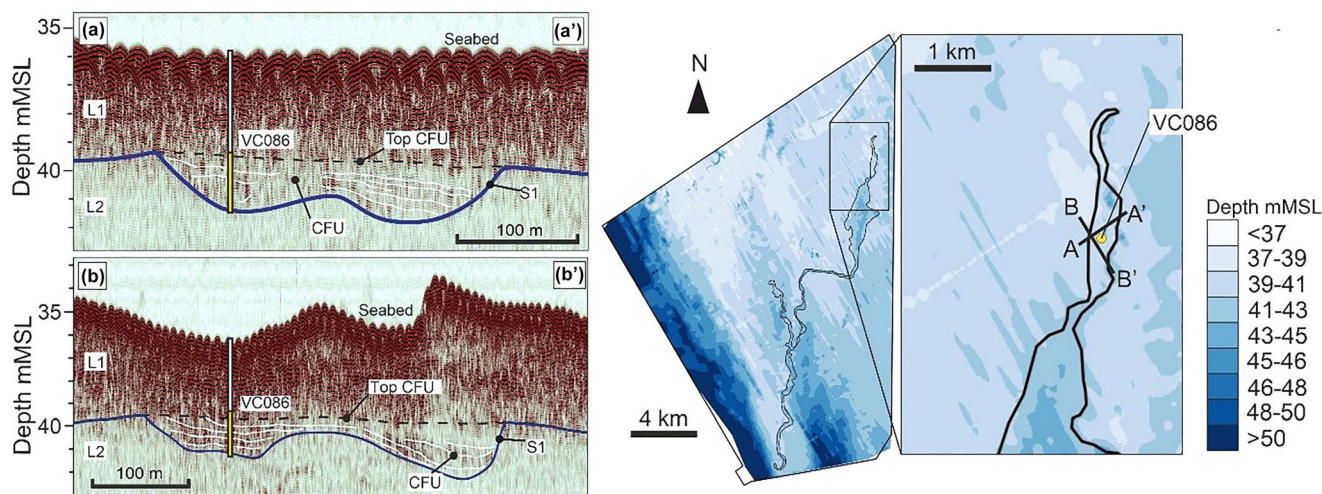
FIGURE 4 Seismic cross-sections showing where vibrocore VC086 intersects the CFU in the northeast of NV West (location shown in map). The seismic character of CFU at VC086 is characterised by low to medium-amplitude seismic reflectors that are parallel and sub-horizontal, draping the channel-form margins. [Color figure can be viewed at wileyonlinelibrary.com]

or is part of the fill of a channel-fill, but is absent where the incisional fill unit (IU) is mapped (detailed below). The depth to the top of the SAU ranges from 37.5 to 40 m MSL, and locally crops out at the modern seabed (Figure 3a). The SAU deepens southeastwardly in NV West but with no clear depth trend observed in Boreas (Figure 5). Locally, the SAU is characterised by multiple high-amplitude, low-frequency seismic reflectors. No clear trend in SAU thickness is observed across the study area. Typically, the SAU reflectors are parallel to seismic reflectors in the underlying Brown Bank Fm. (Figure 5). The spatial distribution of the SAU closely aligns with the thickest parts of the L1 unit. Typically, where L1 is thin the SAU is not present.

3.1.5 | Incision-fill seismic unit (IU)

The incision-fill seismic unit (IU) differs from CFU in both fill character and planform geometry. In NV West, the IU is irregular in planform (ranging from strongly elongate to sub-circular), and <2.4 km wide. In Norfolk Boreas, the limited reflectivity means that differentiating between the IU and CFU is difficult. This is complicated by the distribution of the two seismic units. Locally, low-aspect-ratio channel-forms widen and then narrow along their length to resemble the irregular planforms of the IU (Figure 6). SAU is never observed within or above the IU, but where the SAU is immediately adjacent to the IU, the SAU terminates abruptly at the IU margin. Multiple seismic facies characterise the infill of the IU (Figure 6). Complex fills in NV West (Figure 6a) and Boreas are characterised by stacked progradational, draped and transparent fills. Where progradational fills are observed, reflectors tend to dip southward. The IU is distinguished from the overlying SB unit by an abrupt change in seismic facies character and/or truncation of seismic reflectors.

3.1.6 | Seabed bedforms (SB)

The seabed bedforms unit (SB) overlies the SAU, CFU and IU. The thickness of the SB unit is highly variable across the study area. S1

crops out at the seabed in the west and central southern areas of NV West, and in the troughs between the north–south-orientated sand banks in Boreas. At these locations, there is only a thin veneer (<0.4 m) of sediment characterised by continuous to discontinuous, high-amplitude seismic reflectors (Figure 3). The north–south-orientated sandbanks (Figure 7) with superimposed dune-scale bedforms (up to 4 m high) mark the thickest SB unit (up to 8 m thick). In these areas, the seismic character of the SB unit is often low amplitude to transparent, but dipping seismic reflectors are present, corresponding with the dip of the lee face of the sandbanks.

3.2 | Sedimentary analysis

The eight vibrocores logged in detail and twelve assessed from photographs intersect three of the seismic subunits (CFU, SAU and SB) of L1. None of the available vibrocores intersected the IU. The CFU and SAU overlie the S1, and locally the SAU forms part of the channel-fill, so are broadly contemporaneous, although the SAU is mapped separately (Figure 2, inset to Panel (a-b)). The SAU is not identified within the IU and is therefore considered to be older. The resolution of the seismic reflection data means there is some uncertainty in directly correlating between seismic units and sedimentary facies present within the cores, particularly if the units are relatively thin or transitional in nature.

3.2.1 | Channel-fill unit (CFU)

The channel-fill unit (CFU) is sampled in vibrocores VC086 and VC074 (Figure 8; locations shown in Figure 1) and shows a sharp basal contact with S1 (and by association with the L2 unit mapped in Eaton et al. (2020)) and is overlain by shallow marine sands (SB unit). In VC086, the CFU interval is characterised by sedimentary facies Ssh, which comprises dark grey fine-to-medium silty sand with abundant shell fragments distributed throughout. By contrast, in VC074, the CFU comprises fine-grained sand (sedimentary facies Sfs), which increases in organic content, with components distributed as horizons
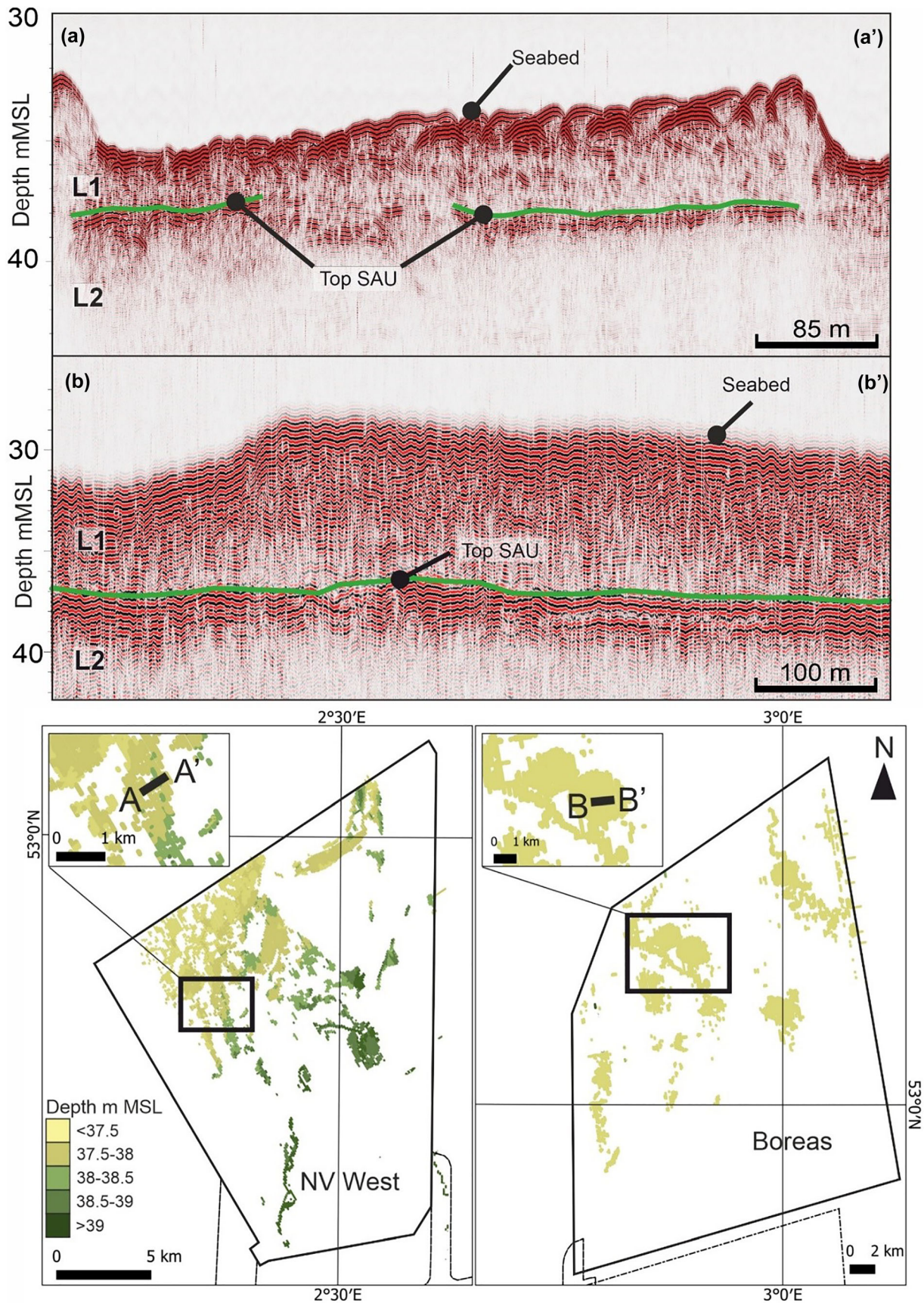
FIGURE 5 Example seismic reflection cross sections of the SAU in NV West and Boreas, which are indicated with a dashed line. The mapped top SAU surface is coloured in depth below sea level. Profiles (a) and (b) show examples of the SAU unit (which correspond to the peats observed in vibrocores) and the variation in thickness (number of seismic reflectors). In both examples, the SAU unit is overlain by a seabed bedforms (SB) unit. [Color figure can be viewed at wileyonlinelibrary.com]
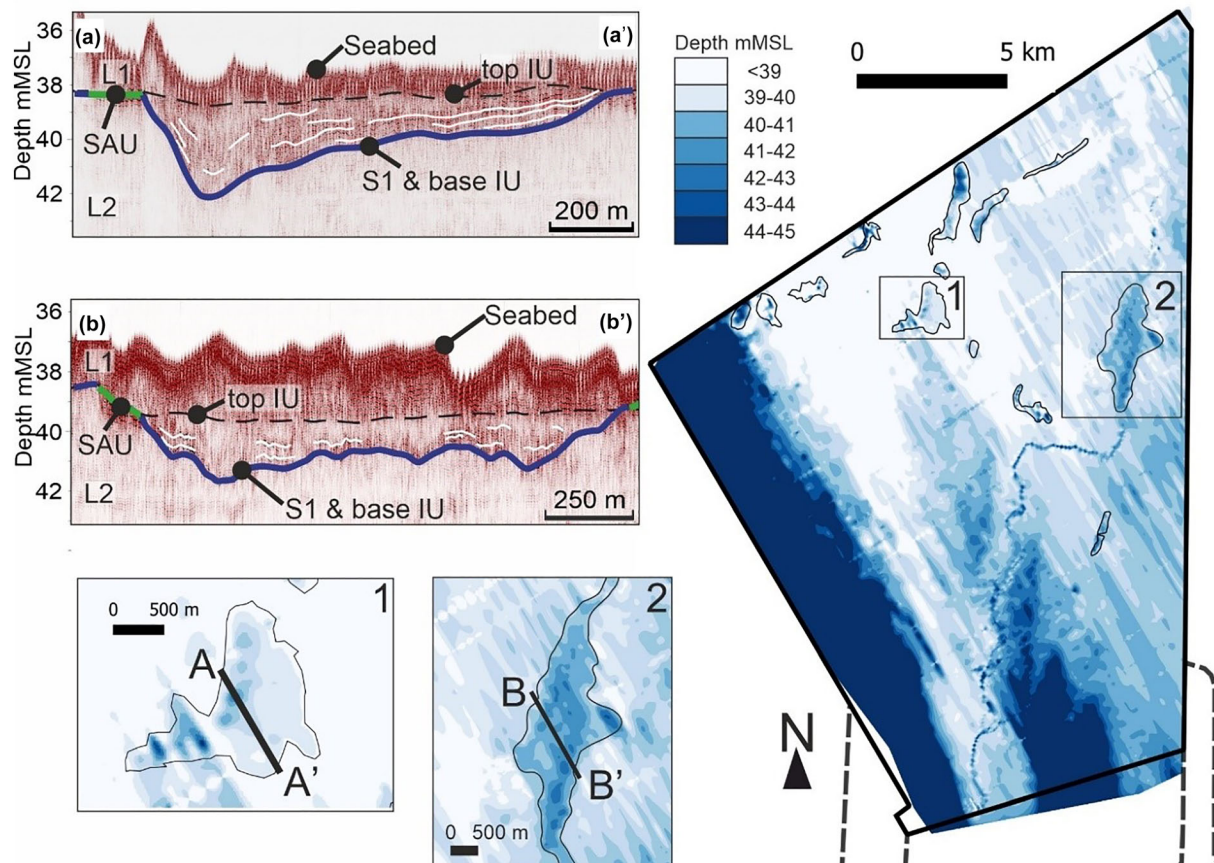
FIGURE 6 Seismic sections showing examples of the incisional seismic unit (IU). A range of seismic fill types characterises the incision-fill seismic unit. (a) Seismic section shows an incision surface with a chaotic fill character and dipping reflectors. Along the northern margin of this feature is the SAU, which is truncated by the IU. (b) Seismic section shows an incision surface that forms part of the CFU interpretation, although its irregular planform resembles IU. Dipping, sub-horizontal and transparent seismic fill characterise this feature. The mapped S1 surface in NV West is shown in the main map on the right, with inset maps showing the location of panels 1 and 2. [Color figure can be viewed at wileyonlinelibrary.com]

and/or lenses through the overlying sedimentary facies, an organic-rich muddy sand (sedimentary facies Sso).

3.2.2 | Seismic anomaly unit (SAU)

The SAU has been identified in seven vibrocores in NV West and Boreas. SAU comprises peat (sedimentary facies Pt), organic-rich sands (Sso) and silts and clays (Cl). In VC028, VC032, VC075, VC080, VC081 and VC088, Pt is underlain by a grey to light-brown silty-clayey sand, which sharply overlies S1 and the L2 unit (Figure 9). In VC039 and VC085, the Pt overlies a light-grey clayey-silty sand grading to a dark-brown sandy mud (which in VC039 is ^{14}C dated by Wessex Archaeology (2019b) to 12,616–12,004 cal. yr BP (Table 1)). In VC074 (Figure 8) and VC081 (Figure 9), organic-rich sands (Sso) underlie the Pt. Locally, the increased organic content through the Sso makes a correlation between the top of the CFU and the base of the SAU in the seismic reflection data and the sedimentary units present within the cores challenging.

The peat observed in the cores is dark brown, humified and amorphous, with wood fragments present in VC028. The peat is overlain by a thin (<0.1 m) organic-rich dark brown clay in VC028, VC074 and VC085. The contact between Pt and the overlying SB unit is sharp in cores VC039, VC075, VC080 and VC085, and is convolute in cores VC028, VC074 and VC076 where the SB unit incorporates organic-

rich components and/or clay. In VC032, the Pt transitions upwards into a clayey silt with thin ripple cross-laminated sands. A ^{14}C age of 10,506–10,175 cal. yr BP exists from this layer (Table 1) but given its relatively old age compared to the dates from the peat below (Figure 10) and the nature of the unit, it is considered by Wessex Archaeology (2019a) to contain reworked carbon.

Minimum age for the onset of peat deposition is given by basal ^{14}C dates obtained by Wessex Archaeology (2018a, 2018b, 2019a, 2019b) from six cores (Figure 10 and Table 1). These ages are derived from mixed macrofossil assemblages of freshwater seeds and leaves, except for the lower date in VC032, which is based upon a bulk sediment sample. Maximum ages are obtained from similar organic material found at the top of the peat layers, although these may not represent the youngest age of formation due to the potential for erosion during marine transgression (Figure 10). In VC074 and VC032 further dates are reported from within the peat profiles, which in VC074 show a slight age reversal with respect to the lowermost date and are as a result considered unreliable by Wessex Archaeology (2019b). Overall, the ^{14}C ages indicate peat formation in Boreas and NV West occurred during climatic warming following the Last Glacial period and into the Early Holocene from c. 13.9 to 9.5 cal. yr BP. The seismic stratigraphic relationship of the peat and the CFU, with the peat underlying, overlying and intercalated with the CFU (Figures 2 and 11) points to peat accumulation being contemporaneous with the incision and fill of the channels. This is supported by the presence of
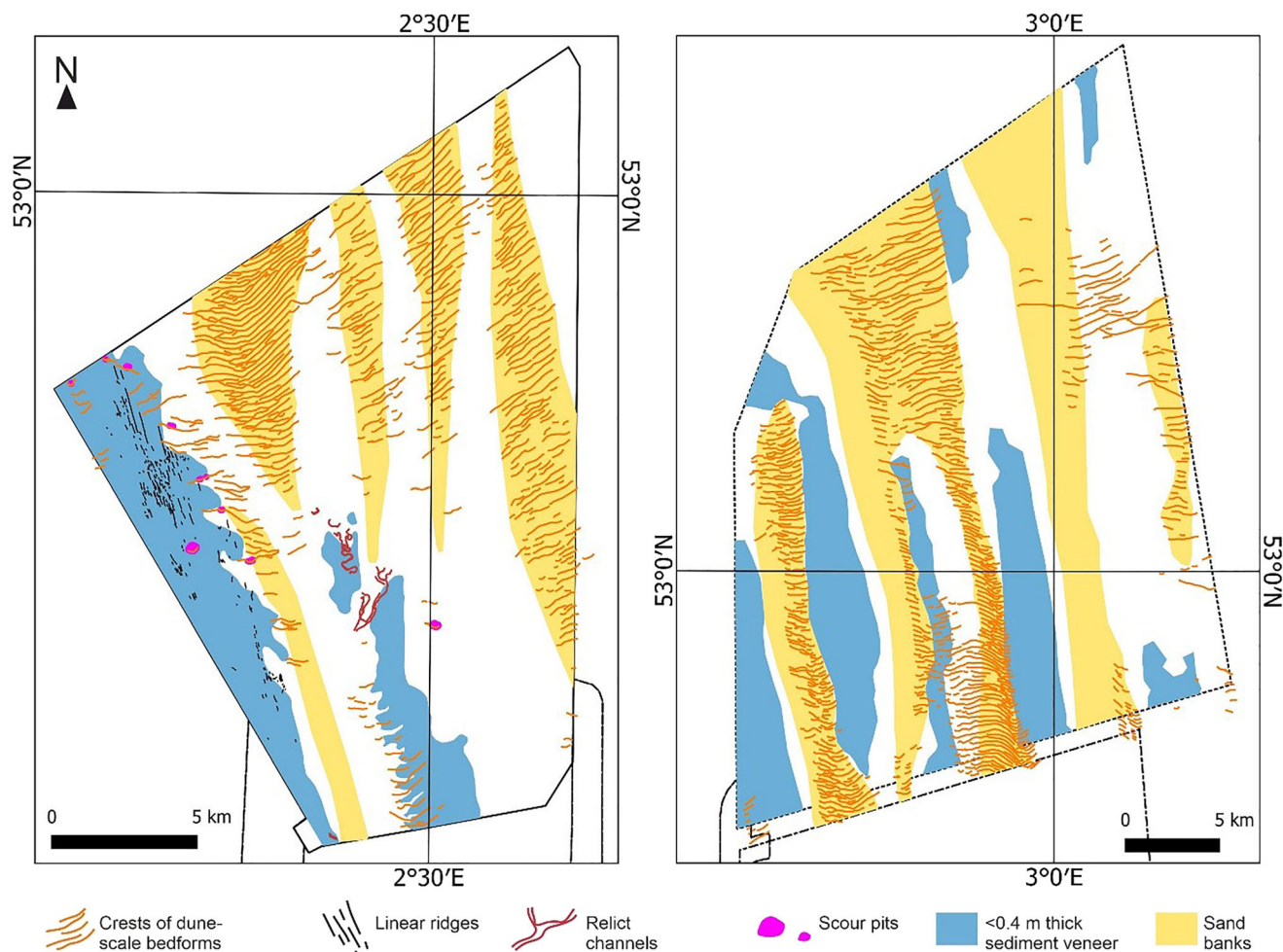
FIGURE 7 Key seabed features interpreted from bathymetry data and SBP seismic in NV West (left) and Boreas (right). The crests of the dune-scale bedforms are superimposed over north–south trending sand banks. Where only a thin veneer of seabed sediment is present (blue) the L1 unit crops out at the seabed. Relict channels (CFU) and scour pits associated with dunes and linear ridges are also shown. [Color figure can be viewed at wileyonlinelibrary.com]

pollen in the peats typical of vegetation of this time period (Wessex Archaeology, 2019a, 2019b).

3.2.3 | Seabed bedforms unit (SB)

All vibrocores sample from the seabed downwards and therefore give good control of the SB unit thickness. The thickness of the SB unit in the cores is highly variable (0.12 to >6 m), with the thickest intersections corresponding to sandbanks. Along the western margin of NV West (VC071 and VC072), a very thin SB unit is present (<0.2 m thick). In VC077 and VC118, no SB unit is observed, with the L2 unit (Brown Banks Fm.) cropping out at the seabed. In cores VC070, VC078, VC084, VC086 and VC115, the facies comprise a golden-brown, well-sorted medium sand with rare, fragmented shells (Sm), with some silt and clay at the base, and the fine-grained fraction decreasing upwards, which is characteristic of sandbanks (Roos et al., 2007; Van Oyen et al., 2013). In VC078, coarse-grained sand with gravel and pebbles (<4 cm diameter) marks the base of the SB unit. In VC081 and VC085, organic-rich clayey horizons are present within the SB unit, and these correspond to dipping seismic reflectors within the large seabed sandbanks.

3.3 | Cone penetration tests (CPTs)

Available CPTs intersect the SAU, CFU and SB seismic units, but not the IU.

3.3.1 | Channel-fill seismic unit (CFU)

Two CPTs penetrate the CFU (Figure 11), and their character is markedly different, supporting the variable characteristics of the CFU identified in the seismic data. CPT074 intersects the margin of the CFU in the southwest of NV West and coincides with the mapped SAU (Figure 11). Differentiating between the Pt and Sso sedimentary facies using only the CPT data is challenging. There is a clear deflection in CPT parameters (friction ratio and cone resistance) at the seismically mapped base of the channel-fill unit and at the top of the SAU, but the change in sedimentary facies is not clearly identified in the CPT (Figure 11). The CPT parameters support a channel-fill unit composed of silty sand to sandy silt with some organic-rich clays (Robertson, 1990), corresponding to sedimentary facies Sso. CPT086 intersects the CFU in the northeast of NV West and has a low friction ratio (<1) and high cone resistance (>3) compared with CPT074, supporting the
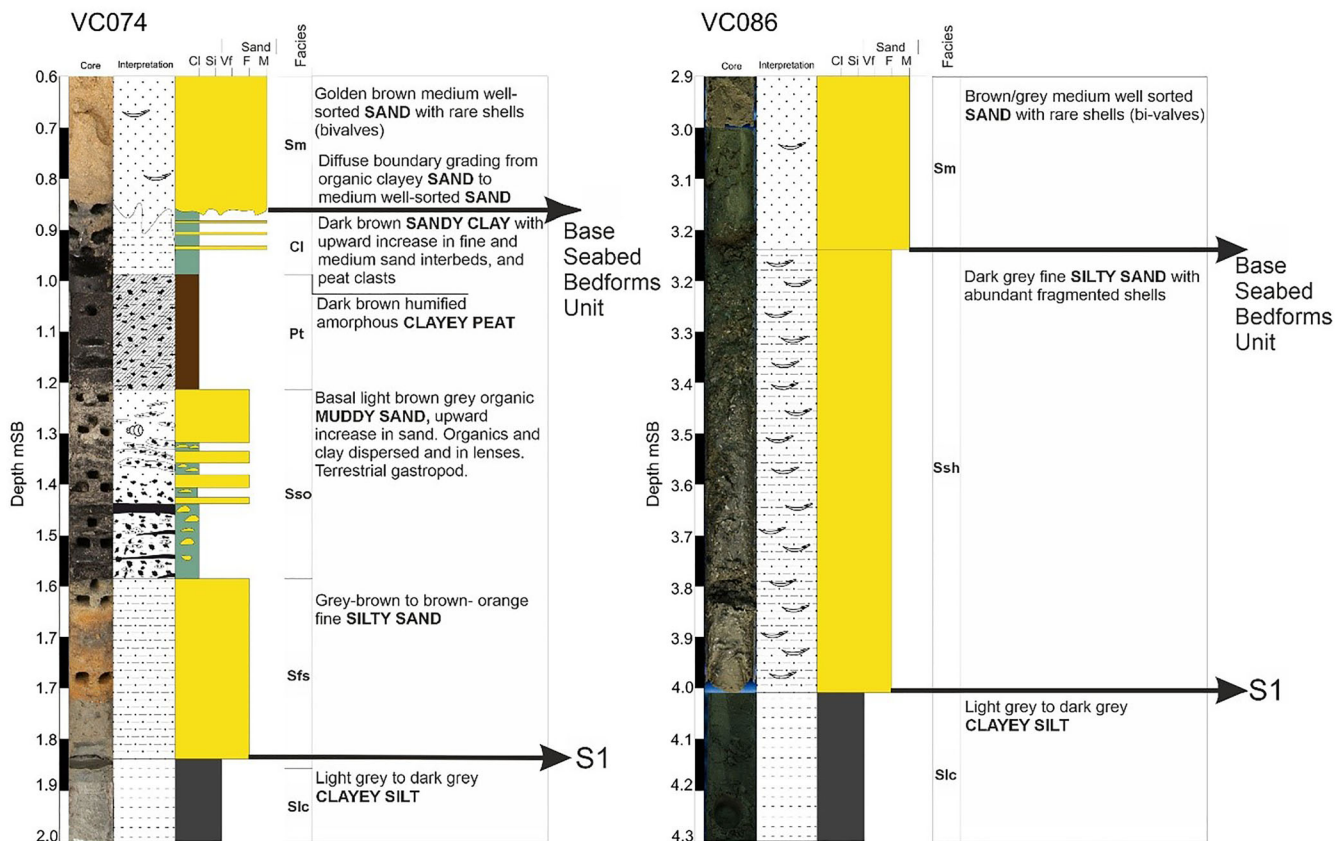
FIGURE 8 Summary of vibrocores that intersect the channel-fill seismic unit (CFU) and seismic anomaly unit (SAU) which sits above S1 (and Eaton et al. (2020) L2) and below the base of the shallow marine sands (below as depth in meters from the seabed (SB)). VC074 is located in the southwest of NV West (Figure 1), and samples the margin of the CFU and is overlain by organic-rich sands and peats (corresponding to the SAU). VC086 samples the CFU closer to the channel axis in the northeast of NV West (Figure 1). The channel-fill here contrasts with that in VC074 and is composed of shell-rich silty sand. [Color figure can be viewed at wileyonlinelibrary.com]
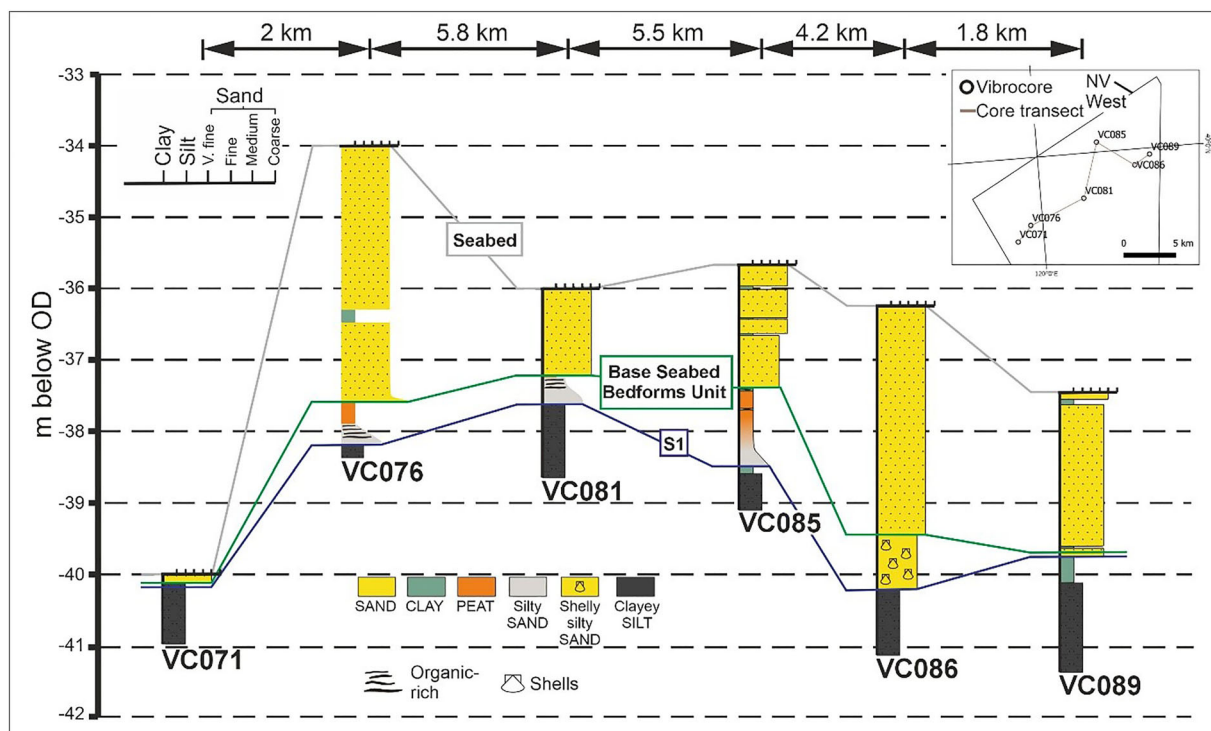
FIGURE 9 An illustrative vibrocore transect through NV West showing the correlation of seismic units and lithostratigraphy observed in the cores. [Color figure can be viewed at wileyonlinelibrary.com]
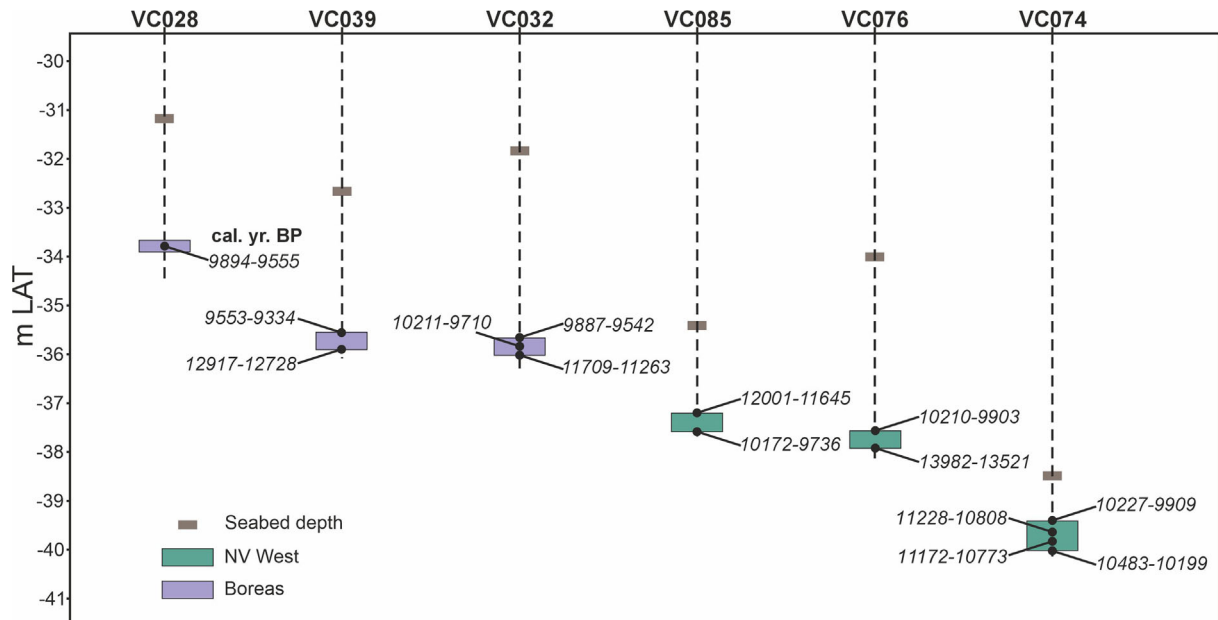
FIGURE 10 Radiocarbon dates from six peat layers present in vibrocores collected from NV West and Boreas (detailed in Table 1). Dates calibrated with IntCal20 (Reimer et al., 2020). [Color figure can be viewed at wileyonlinelibrary.com]
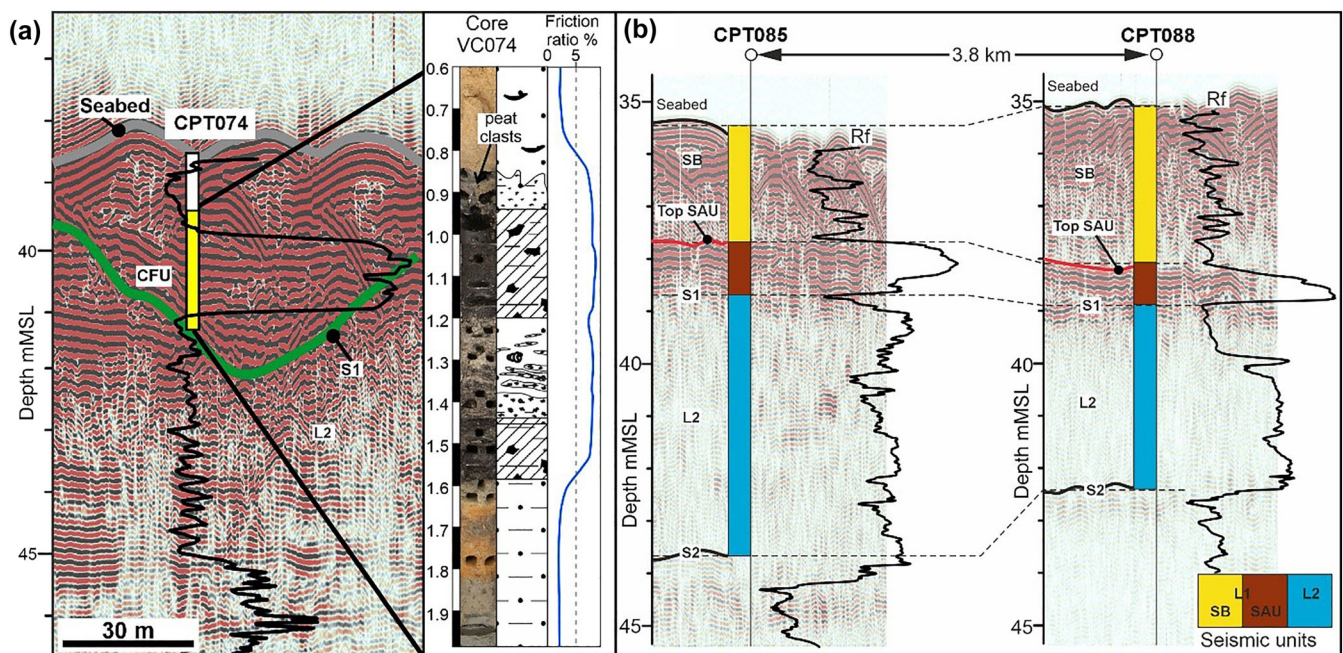
FIGURE 11 Calibration of seismic, core and CPT data. CPT parameter (Rf = friction ratio) overlain in black. (a) VC/CPT 074, with vibrocore path overlain on the seismic data. Yellow indicates the cored unit with the organic-rich interval, including peat within the channel-fill unit (CFU). Note the peat clasts in the overlying sand. See Figure 8a for the core log. (b) CPT 085 (see Figure 9 for core log) and 088 to show the clear response in Rf of the seismic amplitude unit (SAU). SB = seabed bedforms unit, S1 = surface 1, L1 = seismic unit 1, L2 = seismic unit 2. [Color figure can be viewed at wileyonlinelibrary.com]

interpretation of a sand-rich unit. This corresponds to sedimentary facies Ssh, a silty sand with abundant shell fragments (Figure 8).

3.3.2 | Seismic anomaly unit (SAU)

A high friction ratio (Rf; >5%) and low cone resistance (Qc; <1 MPa) occurs through the SAU, which corresponds to an organic-rich clay or peat (Robertson, 1990), consistent with the Pt facies observed in the

vibrocores (Figure 11). This provides confidence that the CPTs are a useful guide as to the presence of the SAU in seismic interpretation where core validation is not available.

3.3.3 | Seabed bedforms unit (SB).

The thickness of the SB unit is well-constrained using CPT data, with a clear change in Rf and Qc seen at the base of the SB unit

corresponding to marked lithological changes observed in the vibrocores from peats, silts/clays or organic-rich sands to marine sands (Figure 11). The SB unit generally has low Rf (<1) and relatively high Qc (10), which supports a sand-rich unit. The character of the CPT shows some variation with small peaks in the CPT parameters (Rf ~ 1.15). The CPTs that record a variable character in the SB unit penetrate sandbanks.

4 | DEPOSITIONAL HISTORY

We integrate the seismic reflection, core and CPT data, alongside information provided from published ^{14}C ages and palaeoenvironmental analyses (Wessex Archaeology, 2019a, 2019b), to propose a depositional history for the postglacial landscape of the study area. Together the results suggest a temporal transition from a fluvial-dominated landscape, through a freshwater peatland and coastal plain setting, to a shallow marine system.

S1 is a composite surface with sediments (L1) that abruptly overlie the Brown Bank Fm. (L2) mapped in Eaton et al. (2020). Overall, the S1 surface is low relief and deepens to the south, with channel-forms and incised features in both NV West and Boreas. The longest channel-fill extends NE–SW at least 26 km, and a shorter N-S trending channel extends 4.7 km, and merges with the longer NE–SW channel in the south (Figure 4). In Boreas, the channel-forms are less extensive (<3.5 km in length). Locally, the maximum thickness of the channel-fill is 5 m, and typically <3 m. The main channel form in NV West has a sinuosity of 1.28 over its preserved length (Figure 6) with some tight bends. Overlying and coincident with the channel margins are peats and organic silts/sands observed in the seismic data (the SAU) and cores (Pt sedimentary facies). In the central and northern areas of NV West and Boreas, discontinuous peats overlie the S1 surface.

The distribution of Sso (organic-rich sand) is patchy, and absent in some cores, suggesting erosive processes. In VC074, sharply overlying S1 are sands, silts and clays (sedimentary facies Sso) of the CFU, with the presence of freshwater diatoms (*Aulacoseira granulata*, *A. ambigua*, *Epithemia* sp., *Epithemia turgida* and *Pinnularia major*). The presence of foraminifera and ostracods from the underlying Brown Bank Fm. (L2), suggests there was a reworking of the substrate (Wessex Archaeology, 2018b, 2019b). Particle-size distribution analysis of the Sso facies present in VC076 shows an unimodal distribution (Wessex Archaeology, 2019b). No microfossils are present within this unit in VC076, but under microscope analysis, the grains appear to be transparent and well-rounded, which Wessex Archaeology (2019b) uses to interpret the sediments as water-lain, rather than windblown. Together with the absence of marine microfossils, the presence of *Aulacoseira* species in the same unit in VC074, whose ecological preference is moving freshwater environments (e.g. rivers, well-mixed lakes) (Stoermer & Julius, 2003), and organic remains, Sso most likely represents deposition in a fluvial or shallow lacustrine environment.

Peat that formed between c. 13.9 and 9.5 cal. yr BP (Figure 10) overlies both the S1 surface and the CFU seismic unit. Pollen assemblages through the peat in VC076 suggest that initial peat development (from c. 13.7 ka) occurred in an open woodland dominated by birch, with wetlands forming on low-lying, open ground. The pollen assemblage is then characterised by a herb swamp with some birch woodland, potentially during the Younger Dryas cooling, which was replaced by a pine and hazel-dominated woodland by c. 10 ka BP (Wessex Archaeology, 2019b). In VC028, the pollen assemblages in the peat that formed from c. 9.7 ka BP also shows evidence of a pine-dominated woodland, with increasing influence of hazel and grasslands over time (Wessex Archaeology, 2019a).

The peat, mapped in the SAU (Figure 5), developed in the north of NV West and Boreas as laterally extensive sheets. In contrast, those in the south of NV West formed on the margins of channel forms, where the fluvial channels of the CFU incised into the Brown Banks Fm. (L2). The sinuous nature of the channels, coupled with peat development along their margins, suggests these fluvial systems formed under lower energy conditions over a long time period (>1,000 yrs) (Vandenberghe et al., 2013).

Palaeoenvironmental data recorded through the peat suggest a shift from a well-drained landscape that supported large broad-leaf trees to a wetter fen-bog or wetland landscape as a consequence of rising groundwater levels (Wessex Archaeology, 2019a, 2019b). In VC085, overlying the peat is a silty sandy clay comprising marine foraminifera (e.g., *Ammonia batavus*, *Elphidium macellum*) and ostracods (e.g., *Pontocythere elongata*, *Leptocythere pellucida*), alongside marine and freshwater diatoms, recording a shift in environmental conditions from freshwater to estuarine from c. 11.9 ka (Wessex Archaeology, 2019b). In VC032, the presence of a fine-grained, clay-rich unit above the peat, with ripple-cross lamination, abundant gastropods and a shift from freshwater diatom *Cocconeis placentula* to marine diatom *Paralia sulcata* suggests increasing proximity of marine conditions after 9.7 ka (Wessex Archaeology, 2019a). The sharp contact with the underlying deposits suggests an erosive contact most likely marking a change from a low-energy coastal plain environment with peats and intertidal drainage networks, into a higher-energy shallow marine environment. This shift from a well-drained to waterlogged landscape in the late postglacial, to estuarine and shallow marine conditions is a result of rising RSL during this time (Clark et al., 2022; Shennan et al., 2018).

5 | DISCUSSION

The high spatial resolution and comprehensive dataset used in this study provide insights into the submerged postglacial landscape in the southern North Sea, which evolved during a warming climate following the Last Glacial period and demonstrates the importance of fluvial sedimentary processes, alongside the stratigraphic and landscape response of a low-relief landscape to marine transgression.

5.1 | Peatland palaeoenvironment and preservation

The postglacial landscape of the study area is typified by the development of a sub-arctic peat-forming environment from c.13.9 ka (Figure 10), in association with the development of a postglacial fluvial network. The transition from an arboreal-dominated woodland to a wetter peatland, dominated by herbs, reflects regional climatic warming during the Early Holocene (Emery et al., 2020). The occurrence of saltmarsh taxa (in VC032) subsequently records the

increased proximity of marine conditions, prior to burial by shallow marine sands at c. 9 ka BP (Figures 9 and 10). The elevations of the peat preserved within the two wind farm areas range from −40.5 to −34.5 m MSL (Figures 5 and 10), with some peats directly overlying S1 and others part of the marginal fill of postglacial fluvial channel-fill deposits, characterised by the CFU (Figures 2 and 3).

Given the low-relief landscape and the relatively large area over which the peats are found (Figure 5), these now-discontinuous peats may have once been more extensive across the landscape. Evidence for erosion of the upper peats is seen in VC074 where peat clasts are incorporated into an overlying sand-dominated interval (Figures 8 and 11), in VC076 where peat clasts are seen in the interval overlying the peat, and in VC028 where the upper interval of the peat has sand-rich lenses distributed throughout. The preserved peat distribution is likely a consequence of a number of different mechanisms, including the degradation of peatland in response to autogenic and climatic processes (Morris et al., 2015), and the elevation differences and drainage pattern in the palaeolandscape (Figure 12), which in turn may be more susceptible to fluvial and marine erosion. The abrupt, lateral-stepped terminations at peat margins not associated with channels (Figure 5a)

are also interpreted as an erosive feature, similar to the steep seaward-facing margins (or 'cliffs') of some modern salt marshes and found along the margins of subtidal channels in coastal peatlands (Adam, 2002; Allen, 1989, 2000). This can occur in retrograding systems where the rate of accommodation outpaces the rate of sediment supply (Vis et al., 2015).

5.2 | Postglacial and Holocene channel evolution

The base of the succession within the study area is bounded by the Brown Bank Fm. (L2), most likely deposited between ∼MIS 5d and 4 (Eaton et al., 2020; Waajen et al., 2024). Global mean sea level during MIS 3–2 remained low due to the presence of large ice sheets in the Northern Hemisphere (Gowan et al., 2021), with regional low RSL (Figure 13) resulting in the S1 terrestrial land surface and fluvial geomorphology recorded within the offshore wind datasets. During the timing of the maximum Devensian ice extent along the east coast of England (c. 21.5 yrs BP) the study area would have been <40 km from the ice-front (Clark et al., 2022) where large pro-glacial rivers were
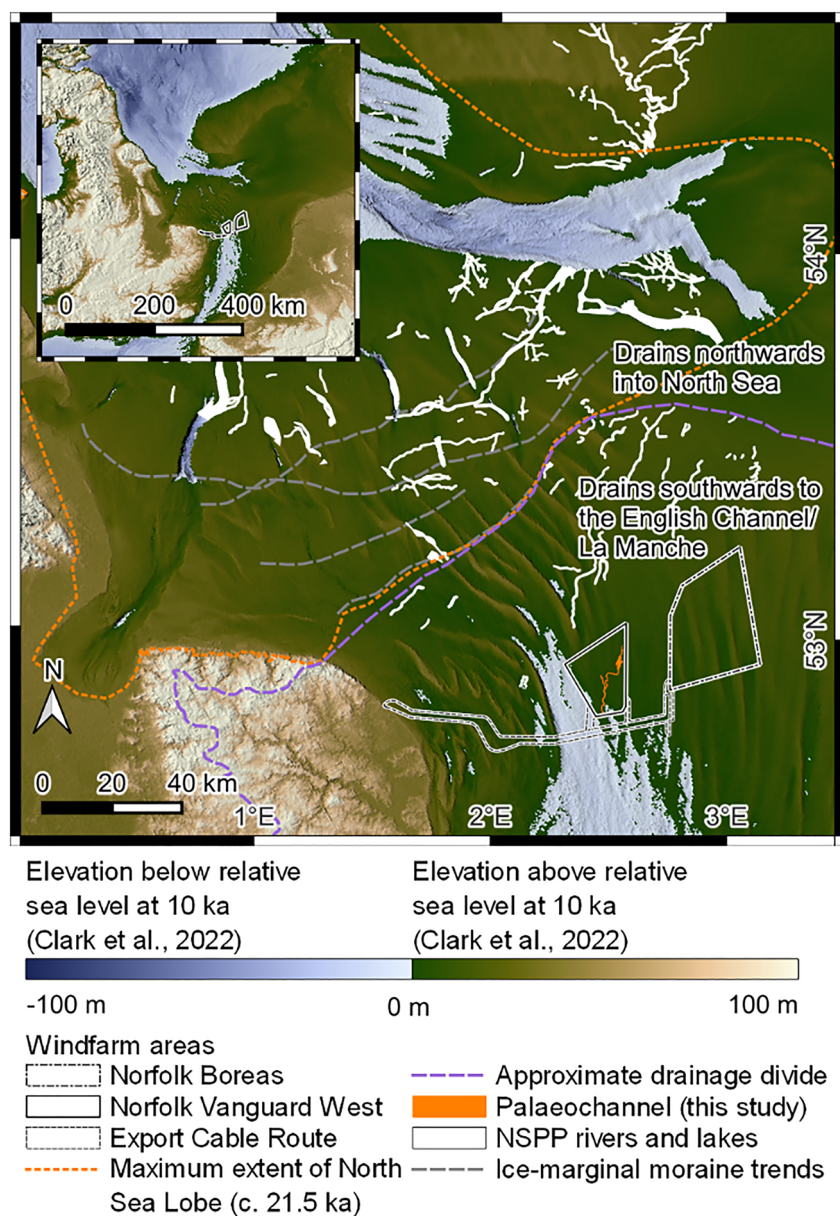
FIGURE 12 Regional context of the palaeochannels observed in NV West, mapped in this study. The southward flow of these channels implies a drainage divide (shown as a purple dashed line) to the north, in contrast to those northward flowing channels (white) mapped as part of the North Sea Palaeolandscapes Project (NSPP; Gaffney et al., 2007). Also shown is the maximum extent of the North Sea Lobe (orange dotted line) and the moraines (grey dashed lines) interpreted by Dove et al. (2017) to mark ice-marginal positions. The topographic colouring shows the glacio-isostatically adjusted elevation of the southern North Sea, and palaeocoastline at 10 ka BP based on the results of Clark et al. (2022), which fit with the ^{14}C ages for the peat formation in the study area (Figure 10; Table 1). [Color figure can be viewed at wileyonlinelibrary.com]

FIGURE 13 Elevation of the western southern North Sea over the last 30 ka, near the study site, based on glacio-isostatic adjustment modelling of relative sea-level change in response to deglaciation of the British-Irish Ice Sheet (adapted from Clark et al. (2022)). The terrestrial landscape lowers as a consequence of relative sea-level rise, during which time there is a period of peatland formation in the study area (yellow band; dates in Figure 10), likely promoted by the rising water table and warming climate, prior to marine transgression c.9 ka BP. [Color figure can be viewed at wileyonlinelibrary.com]
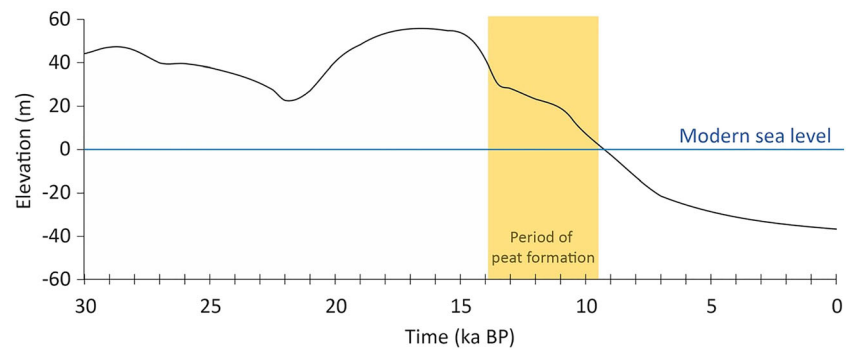
likely present, as a result of seasonal meltwater discharge, over the flat terrestrial landscape (Figure 12). The stacked and multiple seismic fill types of the CFU (and their contemporaneous relationship with the SAU) suggest these channels continued to be occupied through to the Early Holocene as the climate warmed. We interpret a southward drainage direction for the sinuous fluvial network mapped in NV West, which flowed through the freshwater peatlands (Figures 3 and 12). This is supported by the changes in morphology, the tributive planform pattern and the northward closure of fluvial incisions in the study area. Furthermore, the peats (SAU) and S1 dip persistently, albeit gently, southward (Figure 5). Ultimately, the fluvial networks were transgressed due to RSL rise and the northward migration of the shoreline, with overtopping by marine sands recorded in the seismic and core data (Figure 9). The varied depositional nature of the CFU is illustrated in cores VC074 and VC086 (Figure 8), where both intersect the channel-fills but contain different sedimentary facies interpreted to have been deposited in fluvial and marine environments, respectively.

The southward flow of the CFU palaeochannel network in NV West supports drainage into the English Channel/La Manche (Figure 12). Other channels in this region, documented by the North Sea Palaeolandscapes Project (NSPP) (Gaffney et al., 2007) show either a southward drainage close to our study area, or a northward drainage farther north. These differing flow directions support the presence of a drainage divide across the low-relief topography of the southern North Sea during postglacial and Early Holocene subaerial exposure. This drainage divide is roughly coincident with the maximum extent of the North Sea Lobe that occurred at c. 21.5 ka in the southern North Sea (Evans et al., 2019) (Figure 12). The drainage divide follows the ice-marginal moraine sequence interpreted by Cotterill et al. (2017), then diverges from the maximum ice extent position, following a broad and subtle topographic high towards the east. The palaeochannels interpreted by the NSPP (Gaffney et al., 2007) are presented without stratigraphic context but broadly agree with the interpretation of this drainage divide (Figure 12).

The location of the drainage divide suggests subtle variations in topography imparted by the deposition of glacial sediments during the Devensian glaciation-controlled postglacial drainage patterns. Though we lack detailed chronological constraints, it appears that fluvial channel systems that developed after the retreat of the ice sheet followed this broad drainage pattern, as suggested by the CFU palaeochannel network mapped in NV West (Figure 6). In addition, the postglacial drainage network on either side of the drainage divide will have influenced the timing and style of marine transgression from the north and south as the land bridge was inundated by the northern North Sea and the English Channel/La Manche, respectively.

The incisional features identified in the seismic reflection data (the IU) are distinctive in their planform geometry and seismic-fill character compared to the fluvial channel network of the CFU. The seismic character of the IU fills is generally low amplitude with little visible internal structure (Figure 6), whereas the CFU network shows more complex fill patterns with basal high-amplitude seismic reflectors. An exception is where the fill of the IU comprises dipping, draped and truncated seismic reflectors (Figure 6b). Furthermore, the closure of the IU basal surface (S1) in all directions supports a marked difference in origin compared to the CFU that shows sub-parallel erosion surfaces and no closure. Discriminating between the CFU and the IU using seismic reflection data to interpret a differing depositional environment is challenging. Locally, the CFU is overlain by peat (Figure 4a,b) suggesting the channels both pre-date and are contemporaneous with peat formation. In contrast, the incisional features preserve abrupt truncation of peat at their margins and are never observed to be overlain by peat, which supports the development of the incisional unit as either synchronous with, or after, the formation of the fluvial channel network.

The origin of the incisional features is enigmatic given the limited data coverage and lack of similar features documented in the literature. The geographic location and stratigraphic position of these incisional features support formation during a period of RSL rise, likely post-dating the c.10 ka palaeo-coastline position in Figure 12. The Allen (2000) conceptual morpho-stratigraphic model for the evolution of established coastal marshes in response RSL rise leads us to suggest two possible origins: relict tidal drainage channels or relict tidal ponds.

A relict tidal draining origin for the IU is feasible due to the study area experiencing RSL rise such that by c. 9 ka BP sea level had risen sufficiently (Figure 13) for parts of the low-lying marsh to have been within the influence of tidal processes, supported by the presence of salt marsh taxa in VC032. Drainage of flood and ebb waters across the supratidal marsh environment would have been through channels, and water absorption directly through the permeable marsh surface (Allen, 2000). The channels at this stage would have been partially filled with freshwater fluvial deposits (as evidenced in VC074) and would have migrated across the marsh landscape with plant colonisation and peat development on abandoned fills. Continued RSL rise would have led to accretion of intertidal silts and clays on the marsh surface (e.g. VC074, Figure 8), and extension and incision of tidal channels (Rieu et al., 2005). Pre-existing landscape features, such as the fluvial channel network, would either be submerged and/or buried, or repurposed as drainage conduits with the consequent deposition of marine sediments in previously freshwater channels and colonisation by estuarine fauna. At this stage, the down-dip sections

of the drainage channels and associated overbank and peat deposits that were below the elevation of the lowest tides would have been either silted up and buried, or reworked by wave and tidal processes (Allen, 2000). Erosive processes during marine inundation may explain the planform of the incisional units; however, the isolated nature of some of the incisional units remains unclear.

An alternative explanation for the isolated nature of the IU may be that the features represent relict tidal ponds (also known as tidal pools or potholes) that formed during the early Holocene. Tidal ponds form through the failure of the marsh surface to keep pace with the rate of RSL rise (Stevenson et al., 1985), resulting in vegetation loss (Schepers et al., 2016) and enhanced erosion (Baustian et al., 2012), and therefore explain the patchy peatland preservation. Examples of tidal pools are seen in the Mississippi Delta (Ortiz et al., 2017), Chesapeake Bay (Kearney et al., 1988) and the Venice Lagoon (Carniello et al., 2009), and typically occupy 5–15% of the total marsh area (Adamowicz & Roman, 2005; Millette et al., 2010; Wilson et al., 2014). In general, modern tidal ponds are smaller than the IU features, although exceptions are seen in the modern Copper River Delta in Alaska and Lena Delta in Russia, where tidal ponds can be several kilometres wide. Their large size might also be explained as a consequence of the merging of ponds or connection with tidal channels (Wilson et al., 2009, 2010). Alternatively, they may appear large because the basal mapped surface is a time-transgressive stratigraphic surface, rather than a geomorphic surface. More tidal pool-fills may be present in the study area but cannot be identified due to limitations in seismic resolution and line spacing. Furthermore, tidal pond fills could provide a record of palaeoenvironmental change with limited erosion by the overlying marine sands, and we recommend that these features be targeted in future coring programmes to test both these proposed models.

5.3 | Low relief landscape response to relative sea-level rise

The development of the Early Holocene southern North Sea landscape is a function of the rate of RSL rise, sediment budget and accommodation, with the relative importance of the individual factors changing over time (Baeteman & Declercq, 2002). Until c.14 ka, the land surface of this area of the southern North Sea was ∼50 m above MSL (Figure 13; Clark et al., 2022) resulting in channel incision (e.g. Figure 3b), after which the palaeo land surface rapidly lowered as a result of melting of far-field ice sheets and forebulge migration (Bradley et al., 2023). Regional glacial-isostatic adjustment modelling suggests this area of the southern North Sea remained terrestrial until c. 9 ka (Figures 12 and 13), in line with the youngest ^{14}C date from the upper surface of the peat in VC032 (Figures 8 and 10). The rising water table, driven by rising RSL, along with the warming climate and increased precipitation, will have promoted the coeval development of peatland and fluvial networks (Emery et al., 2020; Waller & Kirby, 2021). The relatively older ages of the deeper postglacial peats preserved in NV West, compared to the younger shallow peats in Boreas (Figure 10), and the presence of relict tidal channels or ponds, demonstrates lateral landscape evolution in response to rising RSL and increasing accommodation. In some cases, sediment supply was high enough to preserve estuarine sediments within the channel, most

likely during the earliest and slowest phase of RSL rise (c. 12 ka). However, the erosional upper surface of the peats observed in many cores (Figures 8 and 11), the abruptly terminating SAU that is not explained by channel down cutting, and the patchy peatland preservation (Figure 5) suggests that this was temporally variable, with the fastest rates of RSL rise (>7 mm/yr) during the Early Holocene (Figure 13) outpacing a decreasing rate of sediment supply (Vis et al., 2015). The absence of barrier deposits and/or morphological remnants of barriers is also notable, given they have been documented in the southern Dogger Bank (Emery et al., 2019) and western Denmark (Fruergaard et al., 2015). The elevation of the SAU in Norfolk Boreas is relatively consistent, which may suggest a barrier was present to the south offering protection and allowing the wetland to form in a sheltered setting. At NV West, the elevation of SAU increases towards the north across a natural topographic profile, which is more typical of an open-coast wetland and likely also reflects the micro-tidal range (modelled M_2–0.5–1 m at 8 ka) at this time (Ward et al., 2016). If barriers were present, their absence in the stratigraphic record at both NV West and Norfolk Boreas may reflect the low relief setting and a low sediment supply due to the limited land area (Figure 12). Thus, a combination of rapid RSL rise (Figure 13) and slow sediment accumulation would have resulted in complete reworking through rollover during sea-level rise (Mellett et al., 2012; Storms & Swift, 2003). This process would move sediment laterally landward in pace with rising sea levels, ultimately forming the barrier systems along the modern Norfolk coastline (Andrews et al., 2000). In a low-relief landscape like this, minor changes in RSL impart marked lateral migration of shoreline position and complex flooding patterns (Passeri et al., 2015).

Documenting marine inundation across the low-relief land bridge ornamented with river drainage systems has implications for our general understanding of both submerged and present-day land bridges and barriers, even if the site-specific factors might be different (e.g., rate of glacio-isostatic adjustment). For example, the exposure and submergence of land bridges are crucial for understanding the nature and timing of human migration patterns (e.g., the Bering Straits (Wooller et al., 2018), the Malacca Strait (Adhityatama & Yarista, 2019) and 'Sundaland' (Wurster & Bird, 2016)). The physiographic setting of the early Holocene southern North Sea, a landscape experiencing rising sea levels contemporaneous with decreasing rates of sediment supply (Syvitski, Vörösmarty, et al., 2005; Vis et al., 2015), is a scenario faced by many global deltas and coastlines (Nienhuis et al., 2023). The response of palaeo land bridges and barriers to submergence provides important analogues for future marine inundation over low-relief topography (and potential responses/mitigation) under projected sea-level rise scenarios (e.g., Jutland, Denmark; Cape Cod Peninsula, USA), which makes the southern North Sea a crucial archive of coastal landscape change.

6 | CONCLUSIONS

The acquisition of a high-resolution subsurface dataset optimised to image the shallow subsurface for offshore windfarm ground investigations, alongside core and geotechnical data, has provided a unique opportunity to investigate submerged postglacial landscapes. Following the LGM, this part of the southern North Sea was dominated by

fluvial processes that drained southward. From ~13.9 ka, peats developed on a low-relief coastal plain landscape and continued to develop into the Early Holocene, prior to submergence and burial during marine transgression. Palaeoenvironmental data supports a succession from freshwater peatland through to salt marsh (c. 9.5 ka), in-line with a warming climate and RSL rise throughout the Early Holocene. A contemporaneous drainage divide to the north of the study area is interpreted based on fluvial drainage directions, where a low-relief land bridge separated the North Sea and the English-Channel/La Manche during the Early Holocene. The fluvial channels acted as conduits for marine inundation during the southward and north-eastward migration of the coastline, as the land bridge was inundated by the northern North Sea and the English Channel/La Manche, respectively.

Enigmatic incisional features, separate from the main fluvial networks, are recorded in the seismic reflection data. We propose two possible origins for these features, either relict tidal drainage channels or relict tidal ponds, with their geomorphological profile favouring the latter. These features should be targeted in future coring programmes for potentially continuous palaeoenvironmental archives, offering a sheltered depositional setting with likely minimal erosion.

The present-day preservation of buried postglacial and Early Holocene peats is a result of erosional and degradational processes throughout both the postglacial and Holocene periods and an imbalance between high rates of RSL rise and a sediment supply deficit. Submerged and buried postglacial peats offer insights into the fate of modern low-relief coastal plain wetlands, which are at significant risk of flooding through marine inundation particularly in areas with low sediment flux due to human activities. Through understanding these now submerged analogues, the evolution of modern low-lying coastal plain systems may be better evaluated.

AUTHOR CONTRIBUTIONS

Stephen Eaton: Formal analysis; investigation; methodology; writing—original draft. **Natasha L. M. Barlow:** Supervision; writing—review and editing; **David M. Hodgson:** Conceptualisation; funding acquisition; supervision; writing—review and editing; **Claire L. Mellett:** Supervision; writing—review and editing; **Andy R. Emery:** Writing—review and editing.

ACKNOWLEDGEMENTS

DATA AVAILABILITY STATEMENT

Due to commercial confidentiality, the data presented in this paper are not publicly available.

ORCID

Natasha L. M. Barlow https://orcid.org/0000-0002-2713-2543
Andy R. Emery https://orcid.org/0000-0003-1231-0148

REFERENCES

Adam, P. (2002) Saltmarshes in a time of change. *Environmental Conservation*, 29(1), 39–61. Available from: https://doi.org/10.1017/S0376892902000048

Adamowicz, S.C. & Roman, C.T. (2005) New England salt marsh pools: a quantitative analysis of geomorphic and geographic features. *Wetlands*, 25(2), 279–288. Available from: https://doi.org/10.1672/4

Adhityatama, S. & Yarista, A.S. (2019) Potential of submerged landscape archaeology in Indonesia. *Kalpataru*, 28, 55–71.

Allen, J.R.L. (1989) Evolution of salt-marsh cliffs in muddy and sandy systems: a qualitative comparison of British west-coast estuaries. *Earth Surface Processes and Landforms*, 14(1), 85–92. Available from: https://doi.org/10.1002/esp.3290140108

Allen, J.R.L. (2000) Morphodynamics of Holocene salt marshes: a review sketch from the Atlantic and southern North Sea coasts of Europe. *Quaternary Science Reviews*, 19(12), 1155–1231. Available from: https://doi.org/10.1016/S0277-3791(99)00034-7

Andrews, J.E., Boomer, I., Bailiff, I., Balson, P., Bristow, C., Chroston, P.N., et al. (2000) Sedimentary evolution of the North Norfolk barrier coastline in the context of Holocene sea-level change. In: Shennan, I. & Andrews, J.E. (Eds.) *Holocene land-ocean interaction and environmental change around the North Sea*, Vol. 166. London: Geological Society, Special Publications, pp. 219–251.

Baeteman, C. & Declercq, P.-Y. (2002) A synthesis of early and middle Holocene coastal changes in the western Belgian lowlands. *Belgeo. Revue Belge de géographie*, 2, 77–108. Available from: https://doi.org/10.4000/belgeo.15994

Baustian, J.J., Mendelssohn, I.A. & Hester, M.W. (2012) Vegetation's importance in regulating surface elevation in a coastal salt marsh facing elevated rates of sea level rise. *Global Change Biology*, 18(11), 3377–3382. Available from: https://doi.org/10.1111/j.1365-2486.2012.02792.x

Blum, M.D. & Roberts, H.H. (2009) Drowning of the Mississippi Delta due to insufficient sediment supply and global sea-level rise. *Nature Geoscience*, 2(7), 488–491. Available from: https://doi.org/10.1038/ngeo553

Bradley, S.L., Ely, J.C., Clark, C.D., Edwards, R.J. & Shennan, I. (2023) Reconstruction of the palaeo-sea level of Britain and Ireland arising from empirical constraints of ice extent: implications for regional sea level forecasts and north American ice sheet volume. *Journal of Quaternary Science*, 38(6), 791–805. Available from: https://doi.org/10.1002/jqs.3523

Bristow, C.S., Chroston, P.N. & Bailey, S.D. (2000) The structure and development of foredunes on a locally prograding coast: insights from ground-penetrating radar surveys, Norfolk, UK. *Sedimentology*, 47(5), 923–944. Available from: https://doi.org/10.1046/j.1365-3091.2000.00330.x

Bussi, G., Darby, S.E., Whitehead, P.G., Jin, L., Dadson, S.J., Voepel, H.E., et al. (2021) Impact of dams and climate change on suspended sediment flux to the Mekong delta. *Science of the Total Environment*, 755(Pt 1), 142468. Available from: https://doi.org/10.1016/j.scitotenv.2020.142468

Carniello, L., Defina, A. & D'Alpaos, L. (2009) Morphological evolution of the Venice lagoon: evidence from the past and trend for the future. *Journal of Geophysical Research*, 114(F4), F04002. Available from: https://doi.org/10.1029/2008JF001157

Cartelle, V., Barlow, N.L.M., Hodgson, D.M., Busschers, F.S., Cohen, K.M., Meijninger, B.M.L., et al. (2021) Sedimentary architecture and landforms of the late Saalian (MIS 6) ice sheet margin, offshore the Netherlands. *Earth Surface Dynamics Discussions*, 2021, 1–40.

Clark, C.D., Ely, J.C., Hindmarsh, R.C., Bradley, S., Ignéczi, A., Fabel, D., et al. (2022) Growth and retreat of the last British–Irish ice sheet, 31 000 to 15 000 years ago: the BRITICE-CHRONO reconstruction. *Boreas*, 51(4), 699–758. Available from: https://doi.org/10.1111/bor.12594

Cotterill, C.J., Phillips, E., James, L., Forsberg, C.F., Tjelta, T.I., Carter, G., et al. (2017) The evolution of the Dogger Bank, North Sea: a complex history of terrestrial, glacial and marine environmental change. *Quaternary Science Reviews*, 171, 136–153. Available from: https://doi.org/10.1016/j.quascirev.2017.07.006

Darby, S.E., Appeaning Addo, K., Hazra, S., Rahman, M.M. & Nicholls, R.J. (2020) Fluvial sediment supply and relative sea-level rise. In: Nicholls, R.J., Adger, W.N., Hutton, C.W. & Hanson, S.E. (Eds.) *Deltas in the Anthropocene*. Cham: Springer International Publishing, pp. 103–126. Available from: https://doi.org/10.1007/978-3-030-23517-8_5

Dove, D., Evans, D.J., Lee, J.R., Roberts, D.H., Tappin, D.R., Mellett, C.L., et al. (2017) Phased occupation and retreat of the last British–Irish ice sheet in the southern North Sea; geomorphic and seismostratigraphic evidence of a dynamic ice lobe. *Quaternary Science Reviews*, 163, 114–134. Available from: https://doi.org/10.1016/j.quascirev.2017.03.006

Eaton, S.J., Hodgson, D.M., Barlow, N.L., Mortimer, E.E. & Mellett, C.L. (2020) Palaeogeographical changes in response to glacial–interglacial cycles, as recorded in middle and Late Pleistocene seismic stratigraphy, southern North Sea. *Journal of Quaternary Science*, 35(6), 760–775. Available from: https://doi.org/10.1002/jqs.3230

Emery, A.R., Hodgson, D.M., Barlow, N.L., Carrivick, J.L., Cotterill, C.J., Mellett, C.L., et al. (2019) Topographic and hydrodynamic controls on barrier retreat and preservation: an example from Dogger Bank, North Sea. *Marine Geology*, 416, 105981. Available from: https://doi.org/10.1016/j.margeo.2019.105981

Emery, A.R., Hodgson, D.M., Barlow, N.L., Carrivick, J.L., Cotterill, C.J., Richardson, J., et al. (2020) Ice sheet and palaeoclimate controls on drainage network evolution: an example from Dogger Bank, North Sea. *Earth Surface Dynamics*, 8, 869–891. Available from: https://doi.org/10.5194/esurf-8-869-2020

Evans, D.J., Roberts, D.H., Bateman, M.D., Ely, J., Medialdea, A., Burke, M.J., et al. (2019) A chronology for North Sea lobe advance and recession on the Lincolnshire and Norfolk coasts during MIS 2 and 6. *Proceedings of the Geologists' Association*, 130(5), 523–540. Available from: https://doi.org/10.1016/j.pgeola.2018.10.004

Fruergaard, M., Andersen, T.J., Nielsen, L.H., Johannessen, P.N., Aagaard, T. & Pejrup, M. (2015) High-resolution reconstruction of a coastal barrier system: impact of Holocene Sea-level change. *Sedimentology*, 62(3), 928–969. Available from: https://doi.org/10.1111/sed.12167

Gaffney, V., Finch, S. & Thomson, K. (2007) *Mapping Doggerland: the Mesolithic landscapes of the southern North Sea*. Oxford: Archaeopress.

GEBCO. (2023) *GEBCO 2023 Grid, GEBCO Compilation Group*. Available from: https://doi.org/10.5285/f98b053b-0cbc-6c23-e053-6c86abc0af7b

Gowan, E.J., Zhang, X., Khosravi, S., Rovere, A., Stocchi, P., Hughes, A.L.C., et al. (2021) A new global ice sheet reconstruction for the past 80 000 years. *Nature Communications*, 12(1), 1199. Available from: https://doi.org/10.1038/s41467-021-21469-w

Hackney, C.R., Vasilopoulos, G., Heng, S., Darbari, V., Walker, S. & Parsons, D.R. (2021) Sand mining far outpaces natural supply in a large alluvial river. *Earth Surface Dynamics*, 9(5), 1323–1334. Available from: https://doi.org/10.5194/esurf-9-1323-2021

Hijma, M.P. & Cohen, K.M. (2011) Holocene transgression of the Rhine river mouth area, the Netherlands/southern North Sea: palaeogeography and sequence stratigraphy. *Sedimentology*, 58(6), 1453–1485. Available from: https://doi.org/10.1111/j.1365-3091.2010.01222.x

Karle, M., Bungenstock, F. & Wehrmann, A. (2021) Holocene coastal landscape development in response to rising sea level in the central Wadden Sea coastal region. *Netherlands Journal of Geosciences*, 100, e12. Available from: https://doi.org/10.1017/njg.2021.10

Kearney, M.S., Grace, R.E. & Stevenson, J.C. (1988) Marsh loss in Nanticoke estuary, Chesapeake Bay. *Geographical Review*, 78(2), 205. Available from: https://doi.org/10.2307/214178

McGowan, S.A. & Baker, R.G. (2014) How past sea-level changes can inform future planning: a case study from the Macleay River estuary, New South Wales, Australia. *The Holocene*, 24(11), 1591–1601. Available from: https://doi.org/10.1177/0959683614544055

Mellett, C.L., Hodgson, D.M., Lang, A., Mauz, B., Selby, I. & Plater, A.J. (2012) Preservation of a drowned gravel barrier complex: a landscape evolution study from the North-Eastern English Channel. *Marine Geology*, 315-318, 115–131. Available from: https://doi.org/10.1016/j.margeo.2012.04.008

Mellett, C.L., Hodgson, D.M., Plater, A.J., Mauz, B., Selby, I. & Lang, A. (2013) Denudation of the continental shelf between Britain and France at the glacial–interglacial timescale. *Geomorphology*, 203(100), 79–96. Available from: https://doi.org/10.1016/j.geomorph.2013.03.030

Michum, R.M.J., Vail, P.R. & Sangree, J.B. (1977) Stratigraphic interpretation of seismic reflection patterns in depositional sequences, seismic stratigraphy applications to hydrocarbon exploration. In: Payton, C.E. (Ed.) *Seismic stratigraphy – applications to hydrocarbon exploration AAPG memoires*. Tulsa: American Association of Petroleum Geologists, pp. 117–133. Available from: https://doi.org/10.1306/M26490C8

Millette, T.L., Argow, B.A., Marcano, E., Hayward, C., Hopkinson, C.S. & Valentine, V. (2010) Salt marsh geomorphological analyses via integration of multitemporal multispectral remote sensing with LIDAR and GIS. *Journal of Coastal Research*, 26, 809–816.

Morris, P.J., Baird, A.J., Young, D.M. & Swindles, G.T. (2015) Untangling climate signals from autogenic changes in long-term peatland development. *Geophysical Research Letters*, 42, 10,788–10,797.

Nienhuis, J.H., Kim, W., Milne, G.A., Quock, M., Slangen, A.B.A. & Törnqvist, T.E. (2023) River deltas and sea-level rise. *Annual Review of Earth and Planetary Sciences*, 51(1), 79–104. Available from: https://doi.org/10.1146/annurev-earth-031621-093732

Ortiz, A.C., Roy, S. & Edmonds, D.A. (2017) Land loss by pond expansion on the Mississippi River Delta plain. *Geophysical Research Letters*, 44(8), 3635–3642. Available from: https://doi.org/10.1002/2017GL073079

Passeri, D.L., Hagen, S.C., Medeiros, S.C., Bilskie, M.V., Alizad, K. & Wang, D. (2015) The dynamic effects of sea level rise on low-gradient coastal landscapes: a review. *Earth's Future*, 3(6), 159–181. Available from: https://doi.org/10.1002/2015EF000298

Reimer, P.J., Austin, W.E., Bard, E., Bayliss, A., Blackwell, P.G., Ramsey, C.B., et al. (2020) The IntCal20 northern hemisphere radiocarbon age calibration curve (0–55 cal kBP). *Radiocarbon*, 62(4), 725–757. Available from: https://doi.org/10.1017/RDC.2020.41

Rieu, R., van Heteren, S., van der Spek, A.J.F. & De Boer, P.L. (2005) Development and preservation of a mid-Holocene tidal-channel network offshore the Western Netherlands. *Journal of Sedimentary Research*, 75(3), 409–419. Available from: https://doi.org/10.2110/jsr.2005.032

Robertson, P.K. (1990) Soil classification using the cone penetration test. *Canadian Geotechnical Journal*, 27(1), 151–158.

Roos, P.C., Wemmenhove, R., Hulscher, S.J.M.H., Hoeijmakers, H.W.M. & Kruyt, N.P. (2007) Modeling the effect of nonuniform sediment on the dynamics of offshore tidal sandbanks. *Journal of Geophysical Research - Earth Surface*, 112(F2), F02011. Available from: https://doi.org/10.1029/2005JF000376

Schepers, L., Kirwan, M., Guntenspergen, G. & Temmerman, S. (2016) Spatio-temporal development of vegetation die-off in a submerging coastal marsh. *Limnology and Oceanography*, 62(1), 137–150. Available from: https://doi.org/10.1002/lno.10381

Shennan, I. & Andrews, J.E. (2000) *Holocene land-ocean interaction and environmental change around the North Sea*, Vol. 166. London: Geological Society, Special Publications.

Shennan, I., Bradley, S.L. & Edwards, R. (2018) Relative sea-level changes and crustal movements in Britain and Ireland since the last glacial maximum. *Quaternary Science Reviews*, 188, 143–159. Available from: https://doi.org/10.1016/j.quascirev.2018.03.031

Shennan, I., Coulthard, T., Flather, R., Horton, B., Macklin, M., Rees, J., et al. (2003) Integration of shelf evolution and river basin models to simulate Holocene sediment dynamics of the Humber estuary during periods of sea-level change and variations in catchment sediment supply. *Science of the Total Environment*, 314-316, 737–754. Available from: https://doi.org/10.1016/S0048-9697(03)00081-0

Stevenson, J.C., Kearney, M.S. & Pendleton, E.C. (1985) Sedimentation and erosion in a Chesapeake Bay brackish marsh system. *Marine Geology*, 67(3-4), 213–235. Available from: https://doi.org/10.1016/0025-3227(85)90093-3

Stoermer, E.F. & Julius, M.L. (2003) 15 - Centric diatoms. In: Wehr, J.D. & Sheath, R.G. (Eds.) *Freshwater algae of North America*. Burlington:

Academic Press, pp. 559–594. Available from: https://doi.org/10.1016/B978-012741550-5/50016-7

Storms, J.E.A. & Swift, D.J.P. (2003) Shallow-marine sequences as the building blocks of stratigraphy: insights from numerical modelling. *Basin Research*, 15(3), 287–303. Available from: https://doi.org/10.1046/j.1365-2117.2003.00207.x

Syvitski, J.P.M., Harvey, N., Wolanski, E., Burnett, W.C., Perillo, G.M.E., Gornitz, V., et al. (2005) Dynamics of the coastal zone. In: Crossland, C.J., Kremer, H.H., Lindeboom, H.J., Marshall Crossland, J.I. & Le Tissier, M.D.A. (Eds.) *Coastal fluxes in the Anthropocene: the land-ocean interactions in the coastal zone project of the international geosphere-biosphere Programme*. Berlin Heidelberg, Berlin, Heidelberg: Springer, pp. 39–94. Available from: https://doi.org/10.1007/3-540-27851-6_2

Syvitski, J.P.M., Vörösmarty, C.J., Kettner, A.J. & Green, P. (2005) Impact of humans on the flux of terrestrial sediment to the global coastal ocean. *Science*, 308(5720), 376–380. Available from: https://doi.org/10.1126/science.1109454

Tornqvist, T.E. (1993) Holocene alternation of meandering and anastomosing fluvial systems in the Rhine-Meuse delta (Central Netherlands) controlled by sea-level rise and subsoil erodibility. *Journal of Sedimentary Research*, 63, 683–693. Available from: https://doi.org/10.1306/D4267BB8-2B26-11D7-8648000102C1865D

Van Oyen, T., Blondeaux, P. & Van den Eynde, D. (2013) Sediment sorting along tidal sand waves: a comparison between field observations and theoretical predictions. *Continental Shelf Research*, 63, 23–33. Available from: https://doi.org/10.1016/j.csr.2013.04.005

Vandenberghe, D.A.G., Derese, C., Kasse, C. & Van den Haute, P. (2013) Late Weichselian (fluvio-)aeolian sediments and Holocene drift-sands of the classic type locality in Twente (E Netherlands): a high-resolution dating study using optically stimulated luminescence. *Quaternary Science Reviews*, 68, 96–113. Available from: https://doi.org/10.1016/j.quascirev.2013.02.009

Vis, G.-J., Cohen, K.M., Westerhoff, W.E., Veen, J.H.T., Hijma, M.P., van der Spek, A.J.F., et al. (2015) Paleogeography. In: Shennan, I., Long, A.J. & Horton, B.P. (Eds.) *Handbook of sea-level research*. John Wiley & Sons: American Geophysical Association, pp. 514–535. Available from: https://doi.org/10.1002/9781118452547.ch33

Waajen, I.M., Busschers, F.S., Donders, T.H., Van Heteren, S., Plets, R., Wallinga, J., et al. (2024) Late MIS5a in the southern North Sea: new chronostratigraphic insights from the Brown Bank formation. *Journal of Quaternary Science*, 39, 408–420. Available from: https://doi.org/10.1002/jqs.3592

Waller, M. & Kirby, J. (2021) Coastal peat-beds and peatlands of the southern North Sea: their past, present and future. *Biological Reviews*, 96(2), 408–432. Available from: https://doi.org/10.1111/brv.12662

Ward, S.L., Neill, S.P., Scourse, J.D., Bradley, S.L. & Uehara, K. (2016) Sensitivity of palaeotidal models of the northwest European shelf seas to glacial isostatic adjustment since the last glacial maximum. *Quaternary Science Reviews*, 151, 198–211. Available from: https://doi.org/10.1016/j.quascirev.2016.08.034

Wessex Archaeology. (2018a) *Norfolk Boreas offshore wind farm, Stage 3 Geoarchaeological sampling and assessment*. Sailsbury: Wessex Archeology Ltd.

Wessex Archaeology. (2018b) *Norfolk vanguard offshore wind farm, Stage 3 Geoarchaeological sampling and assessment*. Sailsbury: Wessex Archeology Ltd.

Wessex Archaeology. (2019a) *Norfolk Boreas offshore wind farm, stage 4 Palaeoenvironmental assessment*. Sailsbury: Wessex Archaeology Ltd.

Wessex Archaeology. (2019b) *Norfolk vanguard offshore wind farm, stage 4 Palaeoenvironmental assessment*. Sailsbury: Wessex Archaeology Ltd.

Wilson, C.A., Hughes, Z.J., FitzGerald, D.M., Hopkinson, C.S., Valentine, V. & Kolker, A.S.J.G. (2014) Saltmarsh pool and tidal creek morphodynamics: dynamic equilibrium of northern latitude saltmarshes? 213, 99–115. Available from: https://doi.org/10.1016/j.geomorph.2014.01.002

Wilson, K.R., Kelley, J.T., Croitoru, A., Dionne, M., Belknap, D.F. & Steneck, R. (2009) Stratigraphic and ecophysical characterizations of salt pools: dynamic landforms of the Webhannet salt marsh, Wells, ME, USA. *Estuaries and Coasts*, 32(5), 855–870. Available from: https://doi.org/10.1007/s12237-009-9203-7

Wilson, K.R., Kelley, J.T., Tanner, B.R. & Belknap, D.F. (2010) Probing the origins and stratigraphic signature of salt pools from north-temperate marshes in Maine, USA. *Journal of Coastal Research*, 26, 1007–1026. Available from: https://doi.org/10.2112/JCOASTRES-D-10-00007.1

Wooller, M.J., Saulnier-Talbot, É., Potter, B.A., Belmecheri, S., Bigelow, N., Choy, K., et al. (2018) A new terrestrial palaeoenvironmental record from the Bering land bridge and context for human dispersal. *Royal Society Open Science*, 5(6), 180145. Available from: https://doi.org/10.1098/rsos.180145

Wurster, C.M. & Bird, M.I. (2016) Barriers and bridges: early human dispersals in equatorial SE Asia. *Geological Society, London, Special Publications*, 411(1), 235–250. Available from: https://doi.org/10.1144/SP411.2

Yang, S.L., Zhang, J., Zhu, J., Smith, J.P., Dai, S.B., Gao, A., et al. (2005) Impact of dams on Yangtze River sediment supply to the sea and delta intertidal wetland response. *Journal of Geophysical Research - Earth Surface*, 110(F3), F03006. Available from: https://doi.org/10.1029/2004JF000271

Yu, S.-Y., Törnqvist, T.E. & Hu, P. (2012) Quantifying Holocene lithospheric subsidence rates underneath the Mississippi Delta. *Earth and Planetary Science Letters*, 331-332, 21–30. Available from: https://doi.org/10.1016/j.epsl.2012.02.021